Coordination Chemistry Reviews

Synthesis, functionalization and coordination chemistry of dibenzotetraaza[14]annulenes

Abdul Qaiyum Ramle [a]*, Edward R.T. Tiekink [b]*, Wan Jefrey Basirun [a]*

[a] Department of Chemistry, University of Malaya, 50603, Kuala Lumpur, Malaysia.

[b] Research Centre for Crystalline Materials, School of Medical and Life Sciences, Sunway University, Bandar Sunway, 47500, Selangor Darul Ehsan, Malaysia.

*Corresponding authors: qaiyum@um.edu.my (A.Q. Ramle); edwardt@sunway.edu.my (E.R.T. Tiekink); jeff@um.edu.my (W.J. Basirun)

Highlights

1. The chemistry of the dibenzotetraaza[14]annulenes (DBTAAs) is reviewed
2. The synthetic strategies for the functionalization of DBTAA are summarized
3. Four types of main substituents at the *meso*-positions of DBTAA are categorized
4. A variety of coordination modes in DBTAA complexes are evident
5. The structure-spectroscopic relationships of DBTAAs are outlined

Abstract

This comprehensive review summarizes recent advances in the synthesis and coordination chemistry of dibenzotetraaza[14]annulenes (DBTAAs) reported between 2010 and 2021. Owing to the smaller N_4 donor cavity compared to that of the porphyrin core, it is not surprising that DBTAA offers versatile and unique coordination modes towards metal ions. The structural modification of the DBTAA core allows for the fine-tuning of their spectroscopic properties. DBTAA and derivatives have been utilized across a wide range of research disciplines such as in electronic devices and biological assays. The feasible preparation of ligands and their metal complexes suggests DBTAAs as potential alternatives to porphyrins.

Keywords: DBTAA, core-functionalization, coordination chemistry, spectroscopic properties

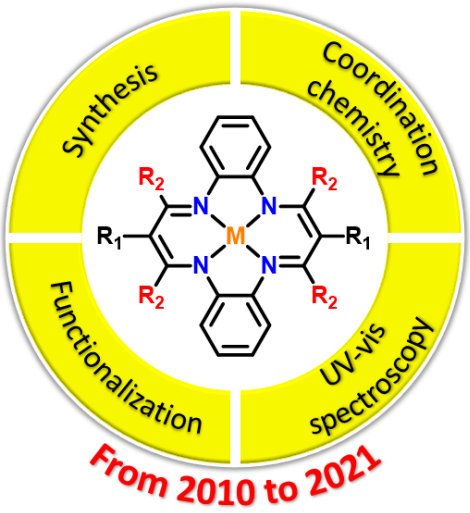

Graphical abstract

Add KODipp below

Abbreviations: COD, 1,5-cyclooctadiene; DBTAA, dibenzotetraaza[14]annulene; Diox, dioxane; Dipp, 2,6-diisopropylphenyl; DME, dimethoxyethane; DMSO, dimethylsulfoxide; DNA, deoxyribonucleic acid; HOMO, highest occupied molecular orbital; K, Kelvin; KCp, potassium cyclopentadienyl; KCp*, potassium pentamethylcyclopentadienyl; KHMDS, potassium bis(trimethylsilyl)amide; LiHMDS, lithium bis(trimethylsilyl)amide; LMCT, ligand-to-metal charge-transfer; Me, methyl; LUMO, lowest unoccupied molecular orbital; MLCT, metal-to-ligand charge-transfer; MOF, metal organic framework; Py, pyridine; RNA, ribonucleic acid; ROMP, ring-opening metathesis polymerization; TMS, trimethylsilyl.

Symbols: M_n, number average molecular weight; M_w, weight average molecular weight; $Đ$, polydispersity index.

1. Introduction

Dibenzotetraaza[14]annulenes (DBTAAs) are a class of macrocyclic compounds that have attracted a great deal of attention mainly due to their being an attractive structural model for naturally-occurring porphyrin derivatives [1, 2]. The unique features of DBTAA give rise to a wide scope of applications such as in dye-sensitized solar cells [3], catalase mimics [4, 5], field-effect transistors [6], as electrical conductors [7, 8], corrosion inhibitors [9], sensors [10], electrocatalysts [11] and as anti-proliferative agents against human tumour cells [12, 13]. Furthermore, DBTAA complexes are efficient catalysts in various organic reactions [14-18]. In addition, they are effectively utilized as host molecules for interactions with fullerenes [19, 20].

The coordination chemistry of DBTAAs is well-known and their notable features with different functionalities have been explored over five decades. Unlike porphyrins, the development of new synthetic methodologies of DBTAA derivatives is typically slow due to the lack of synthetic strategies, functional group tolerance and the availability of precursor compounds. However, owing to several advantages such as economical and short-synthetic routes, acceptable isolation yields, mild-reaction conditions and fine-tuning of the electronic properties, the synthetic work on DBTAA derivatives continues to gather attention owing to the aforementioned desirable properties. Other examples of the imine-type macrocycles which structurally resembles DBTAA are cyclam and [14]cyclidene derivatives but these lack the aromaticity of DBTAA and porphyrins [21-23].

This article focuses on an overview of the practical methodologies for the synthesis of DBTAAs and related compounds reported over the past decade. The synthetic descriptions are categorized into four parts, depending on the type of substituents at the *meso*-positions of the macrocyclic core such as hydrogen, pyridyl, indoleninyl and 2-hydroxy-benzoyl. The versatile core functionalization protocols, metal coordination chemistry and spectroscopic properties are outlined, highlighting their promising future applications. However, the syntheses of precursors such as 1,3-dicarbonyls, vinamidinium salts, metal salts and other structural similarities are beyond the scope of this review.

2. Overview the structural features of DBTAA and porphyrin

As illustrated in Figure 1, the DBTAA and porphyrin macrocycles comprise four nitrogen atoms within the inner core linked by various double bonds. The two N–H protons can be easily deprotonated to form di-anionic ligands for the preparation of metal complexes. However, it is found that the negative charges of DBTAAs are generally delocalized on the 1,3-propanediiminato fragments while they are delocalized throughout the entire ring in porphyrins [24]. With regards to the molecular framework, DBTAA and porphyrin feature of 14- and 16-membered rings, respectively. Structural analyses confirm that the N_4 central cavity size of the DBTAA free ligand is between 1.90 and 1.93 Å, which is approximately 0.1 Å smaller compared to the porphyrin ring. Hence, DBTAA ligands offer a variety of geometric and coordination modes toward numerous metal ions [1]. Interestingly, porphyrins are classified as aromatic systems ($4n$+2) due to their rigid planar structure and full π-conjugation, whereas DBTAAs are not considered as part of the Hückel aromatic system ($4n$) [1, 25]. As such, porphyrin molecules are usually found in a planar arrangement. In contrast, the structural features of DBTAAs are more flexible and can exhibit planar (R_1 = H) [26] or non-planar "saddle-shaped" ($R_1 \neq$ H) conformations [1, 27]. The variation of ligand conformation is caused by steric congestion between the bulky R_1 substituents and the hydrogen atoms of the fused benzene rings. The non-planar shape of the DBTAA ligand has the advantage of having good solubility in many organic solvents due to decreased π-π stacking interactions [28].

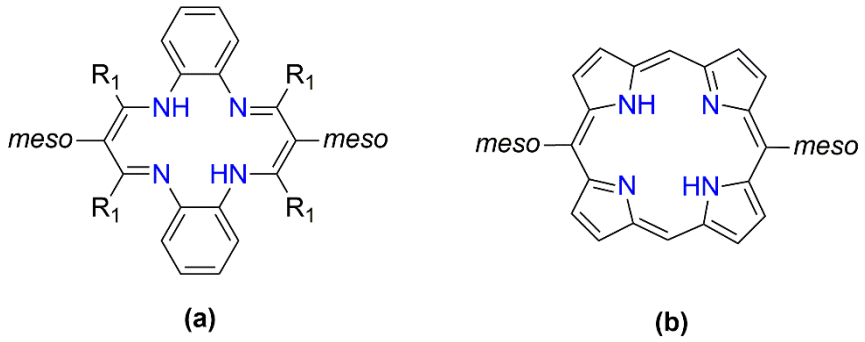

Figure 1. Chemical diagrams of the (a) DBTAA and (b) porphyrin cores.

3. Overview of the synthesis of DBTAA cores

For over half a century, the condensation reaction remains a crucial method for the synthesis of the DBTAA core. In many cases, the reactions are simple and compatible with a wide range of substituents. In 1969, Jäger [29] introduced a template method to synthesize

DBTAA using precursors such as 2,4-pentanedione, *o*-phenylenediamine and $Ni(OAc)_2$ to afford **1** (Scheme 1a). Alternatively, complex **1** could be synthesized from the template reaction of 1,1,3,3-tetramethoxypropane with *o*-phenylenediamine [30-32]. It is observed that in the absence of the $Ni(OAc)_2$ template, the reaction tends to produce 1,5-benzodiazepines [1]. The treatment of **1** with hydrochloric acid followed by basification with triethylamine produces the free ligand **2a** (Scheme 1a) [29]. However, a mixture of regioisomers will be generated when a non-symmetric reactant is employed [33-35]. A versatile synthetic approach to afford the macrocycle core was reported by Honeybourne *et al*. in 1978 [36]. As depicted in Scheme 1b, a non-template condensation reaction between the propynal and *o*-phenylenediamine affords **2b** [36]. However, the metal coordination chemistry of **2b** is not widely explored owing to the insolubility of the ligand. Another example of a non-template reaction is the condensation reaction between substituted vinamidinium salts and *o*-phenylenediamine to generate **2c** (Scheme 1c) [35, 37, 38].

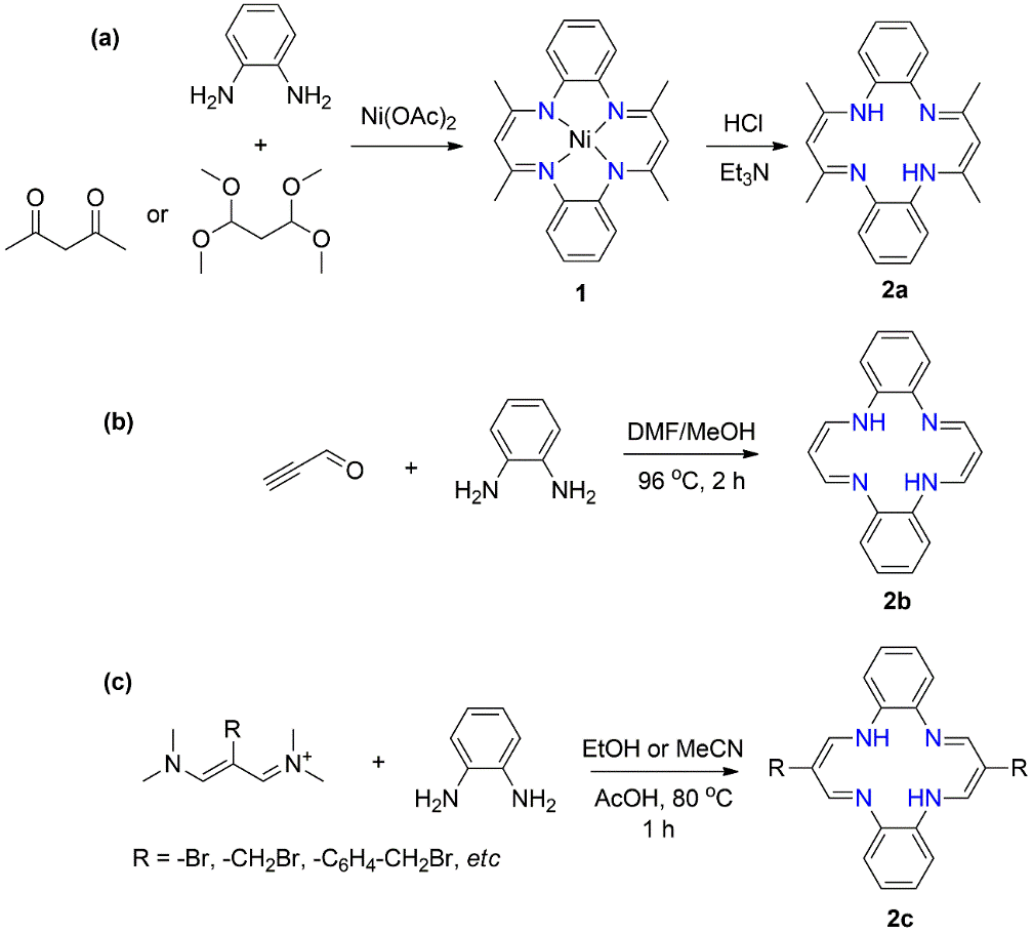

Scheme 1. Synthesis of DBTAAs **1** and **2a-c**.

4. Synthesis and reactivity of *meso*-unsubstituted DBTAA

Shen *et al*. [7] reported the synthesis of germanium-based DBTAA complexes in 2010. The metalation reaction of **2a** with $GeCl_4$ proceeded smoothly to afford **3** in high yield [39] (Scheme 2). The displacement of the axial chlorides with formate afforded **4** in 81% yield [7]. Interestingly, they also discovered that the slow diffusion of **3** into aqueous solutions of disodium 1,4-benzenedicarboxylate or disodium-2,5-dihydroxyl-1,4-benzenedicarboxylate led to the formation of crystalline, one-dimensional coordination polymers **5** and **6**, respectively (Scheme 2) [8]. A representative coordination polymer, namely for **6** is shown in Figure 2. The germanium centre is octahedrally coordinated within a trans-N_4O_2 donor set; this and other crystallographic diagrams presented herein are original and were generated employing DIAMOND [40]. The electrical conductivity of **6** is higher compared to **4** and **5** owing to the presence of the free hydroxyl groups [8].

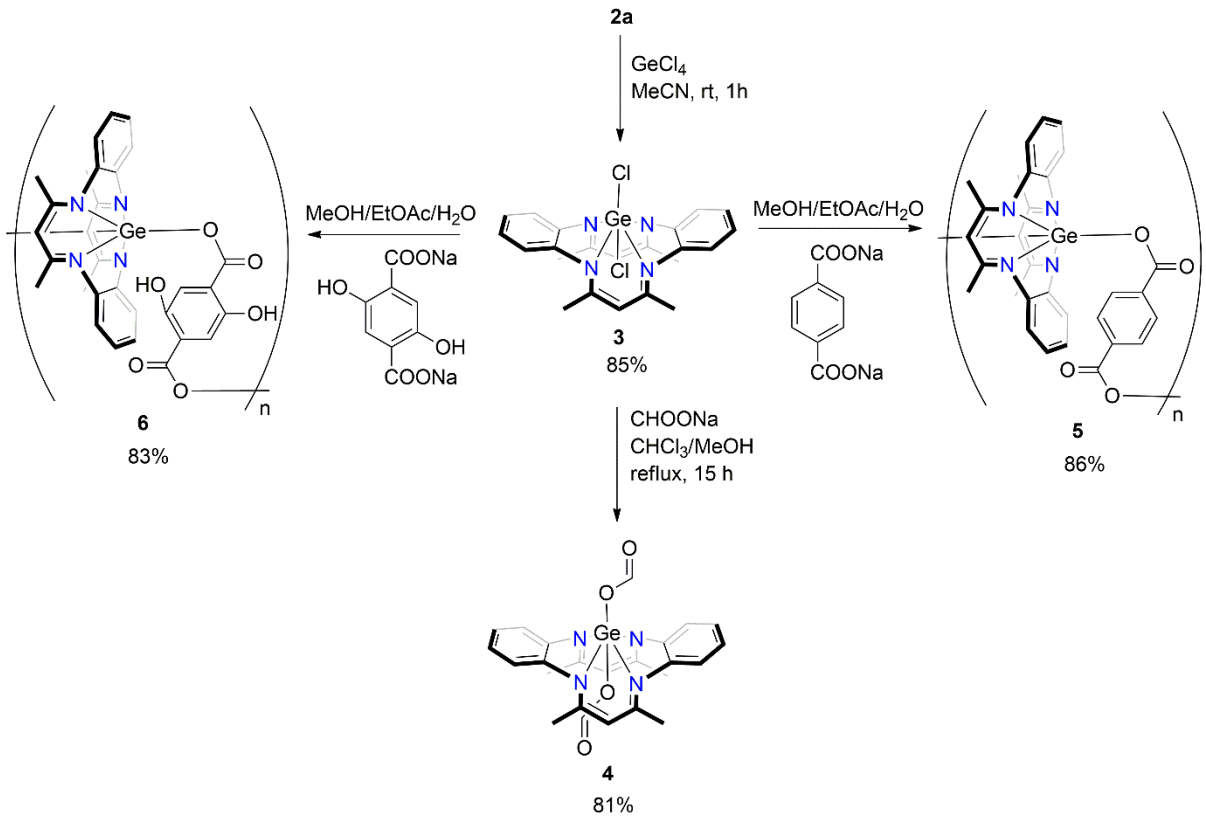

Scheme 2. Synthesis of germanium(IV) DBTAA complexes, **3**-**6**.

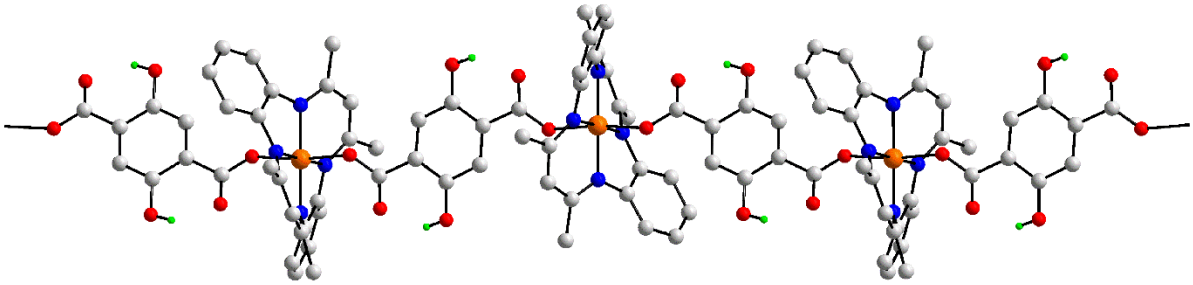

Figure 2. A part of the twisted, one-dimensional coordination polymer **6**. Colour code: metal coordinated to DBTAA, orange; oxygen, red; nitrogen, blue; carbon, grey; hydrogen, green. Non-acidic H atoms are omitted for clarity in all crystallographic diagrams.

Weare *et al*. [41] reported the synthesis of several heterodimetallic complexes based on the DBTAA scaffold. Complex **7** can be synthesized by reacting the free ligand **2a** with $TiCl_4$ in the presence of a base, followed by the addition of aqueous ammonia [42, 43] (Scheme 3). The preparation of **9a-f** was conveniently achieved by refluxing **7** with **8a-f** in acetone (Scheme 3); the molecular structure of the di-cation in **9f** is shown in Figure 3. The crystalline complexes were successfully isolated via the vapour diffusion technique. It was revealed that the Ti=O double bond elongates from [1.653(3) Å] to [1.690(1)-1.704(4) Å] when the oxygen atom is datively bonded to the metal ions forming the heterometallic complexes. The spectroscopic absorption spectra of **9a-f** show strong absorption profiles between 330 and 440 nm. The intensity of the O→Ti ligand-to-metal charge-transfer (LMCT) peak of **9a-f** exhibit red-shifts relative to **7**, indicating that the dative bond connection alters both the Ti–O σ- and π-bonding interactions. As a result, the energy gap between the anti-bonding titanium dπ* orbital and the oxygen pπ*orbital decreases [41].

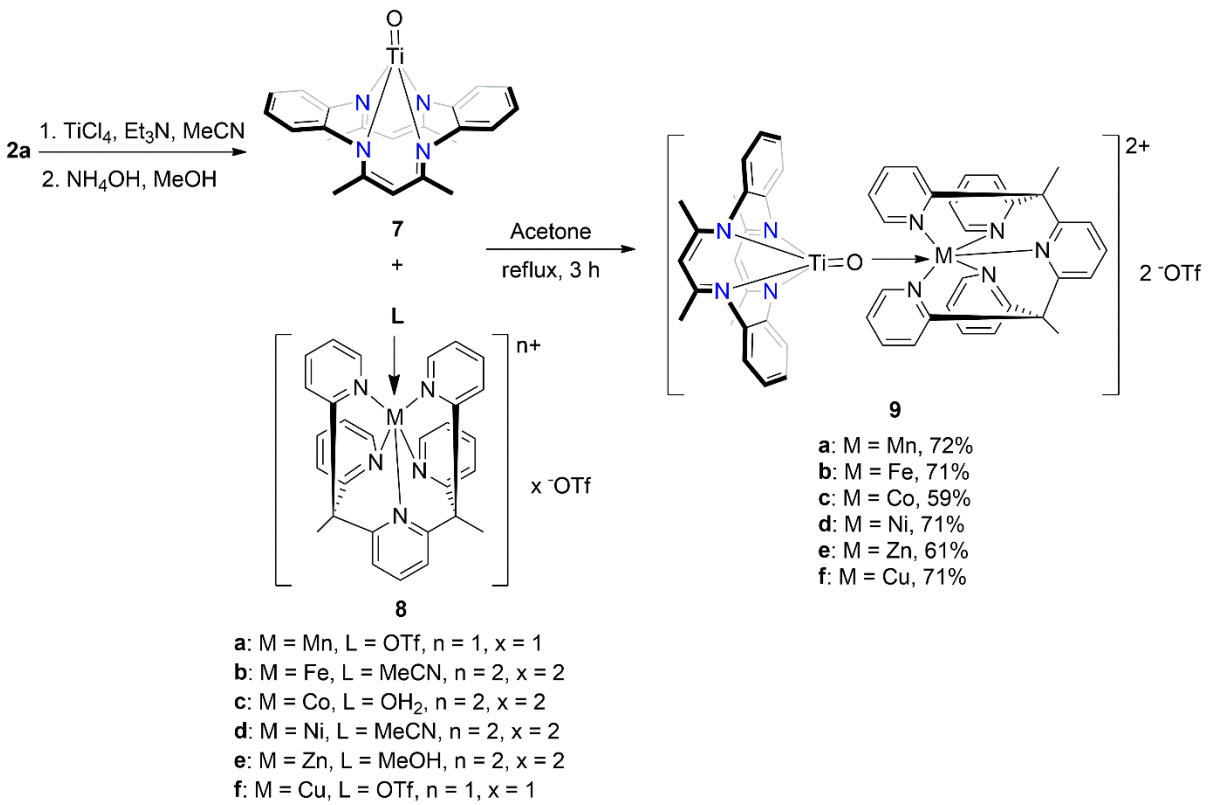

Scheme 3. Synthesis of Ti(IV)=O oxo-bridged heterodimetallic DBTAA complexes, **9a-f**. Note: The Cu(II) ion of **9f** is five-coordinated by an oxo-O and four pyridyl-N atoms of the Py_5Me_2 ligand, which is not in the scheme.

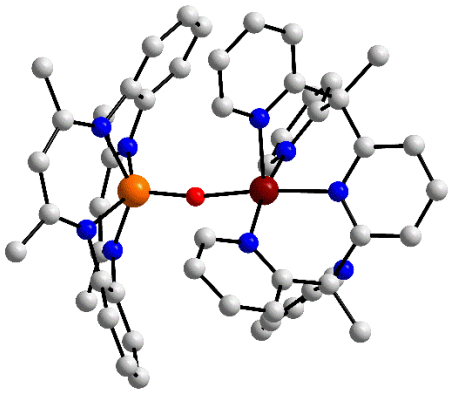

Figure 3. The molecular structure of the di-cation in **9f**, highlighting the square-pyramidal and trigonal-bipyramidal N_4O coordination geometries for the titanium and copper centres, respectively. Additional colour code: copper, brown.

The small core of the N_4 donor cavity of ligand **2a** is ideally suited for coordination to rare-earth elements. Schelter *et al*. [44] synthesized sandwich complexes **10a-b** in reasonable yields by treating the di-potassium salt of **2a** with YCl_3 or $DyCl_3$ in dimethoxyethane (DME) at room temperature (Scheme 4). The crystal structure of complex **10b** was established by X-ray crystallography (Figure 4). The central dysprosium(III) ion is sandwiched by two macrocyclic di-anions and is therefore, coordinated by a N_8 donor set which is close to a cubic geometry. Associated with the aforementioned is a potassium cation which is connected to four nitrogen atoms of a single macrocyclic ligand, as well as four oxygen atoms derived from two DME molecules. The association of the potassium cation with one N_4 face has the result of elongating the Dy−N bond lengths by approximately 0.04 Å. The coordination geometry for the potassium ion is based on a square anti-prismatic N_4O_4 donor set [44]. Complex **10b** is noteworthy for displaying slow magnetic relaxation based on AC magnetic susceptibility measurements.

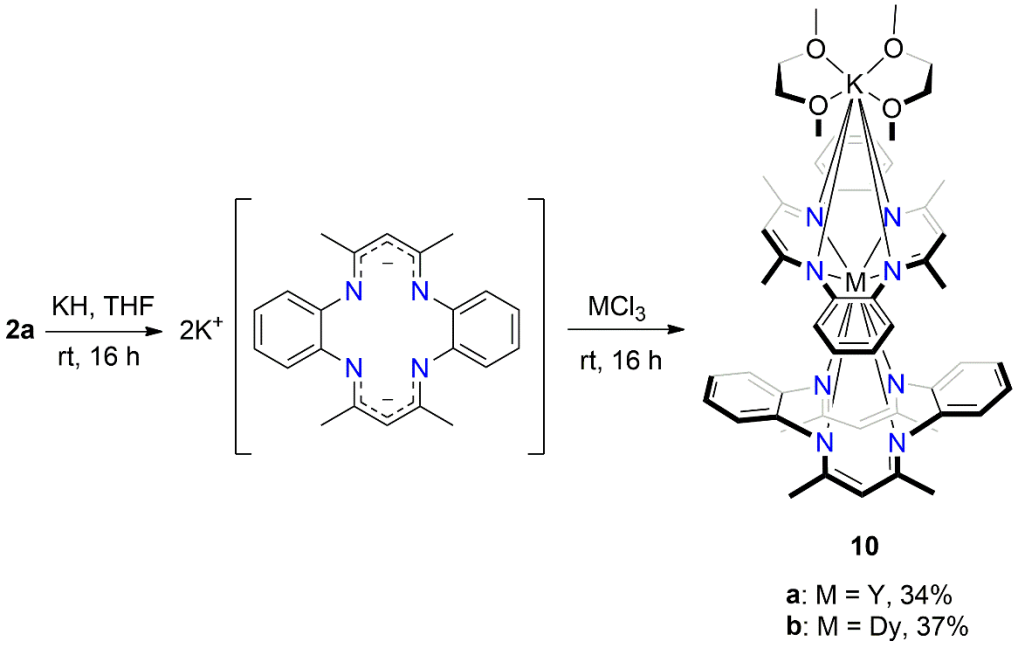

Scheme 4. Synthesis of yttrium(III) and dysprosium(III) DBTAA complexes, **10a-b**.

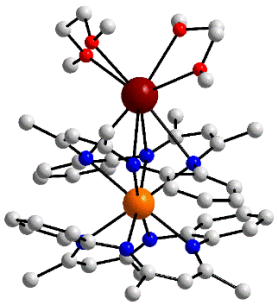

Figure 4. The molecular structure of the neutral aggregate of **10b**, highlighting the sandwiching of dysprosium(III) by two macrocyclic ligands and the cubic geometry defined by the N_8 donor set. The $K(DME)_2$ cation associates with four N atoms of one cubic face with the resulting N_4O_4 donor set approximating a square anti-prismatic geometry. Additional colour code: potassium, brown.

In 2013, Schelter *et al*. [45] also described some coordination chemistry of cerium with DBTAA. Referring to Scheme 5, ligand **11** was prepared according to a template method as described in section 3. The reaction between **11** and $Ce(HMDS)_3$ [46] in warm toluene led to the precipitation of red-brown crystals of **12**. Upon exposure of the crystals to the atmosphere, cerium(III) was oxidized to cerium(IV) resulting in the formation of dark-green crystals of **13** in excellent yield. The structure determination of **13** in solution was successfully elucidated by NMR spectroscopy. Solid-state analysis shows that the central cerium(III) ion of **13** is sandwiched by two tetradentate ligands with the N_8 donor set defining a cubic geometry similar to that of dysprosium(III) in **10b**, Figure 4. The crystal structure of **12** exhibits very similar geometric features to that of **13**. However, there are significant difference between these two complexes with regards to the Ce−N bond lengths. As expected, the Ce−N bond lengths in the cerium(III) complex, ranging from 2.5259(15) to 2.5690(16) Å, are significantly longer than the analogous bond lengths in the cerium(IV) complex, which range from 2.4368(15) to 2.4599(16) Å, in accord with expectation [45]. Cyclic voltammetry analysis of **13** shows a reversible reduction wave at -1.7 V, relative to the ferrocene/ferrocenium, which is attributed to the Ce(III/IV) couple [45].

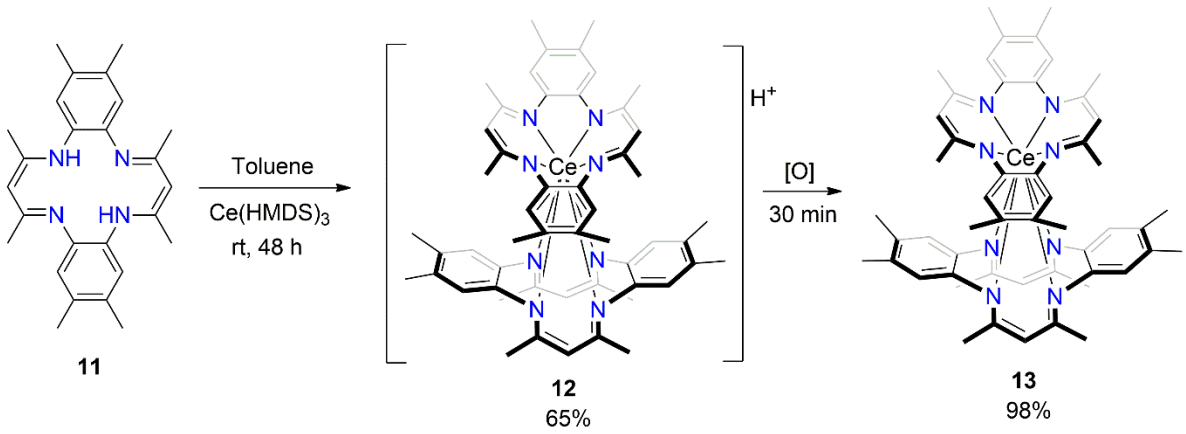

Scheme 5. Synthesis of cerium(III/IV) DBTAA complexes, **12**-**13**.

Wayland *et al*. [47-49] discovered a set of versatile reactions between rhodium and DBTAA. The dimeric rhodium(II) complex **14** was synthesized by refluxing rhodium(II) acetate with **2a** in toluene (Scheme 6) [47]. The pressurized reaction of **14** with CO in benzene afforded the highly light-sensitive product **15**, a bridged di-rhodium(III) carbonyl complex [25]. It was discovered that the reaction of **14** pressurized with a mixture of gaseous H_2 and CO gave the complete conversion into **16** in 24 hours [48]. Dimeric **14** was converted into the heterometallic complex **17** after irradiation with UV in the presence of $[CpFe(CO)_2]_2$ over several minutes. In a similar manner, the reaction of **14** with $[Co(CO)_4]_2$ furnished complex **18**. Interestingly, the X-ray crystallographic analysis of **18** (Figure 5) shows the presence of a semi-bridging carbonyl ligand between the Rh(II)−Co single bond, which occurs due to the donation of the rhodium $d\pi$ orbital into the CO π^* orbital. Complex **19** can also be prepared by the simple mixing of **14** with $[Mn(CO)_5]_2$ under similar conditions as for the preparation of **17** and **18** [49].

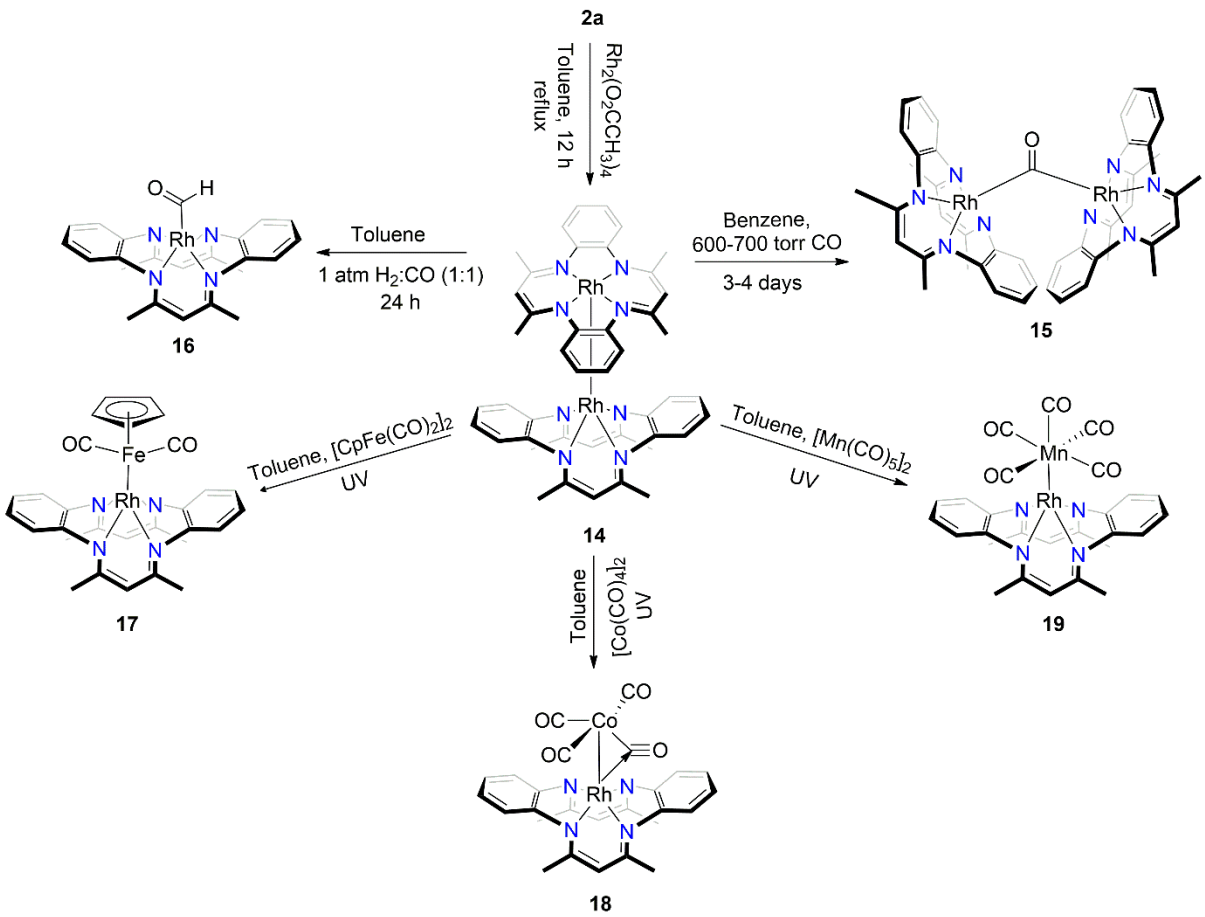

Scheme 6. Synthesis of rhodium(II/III) and heterobimetallic DBTAA complexes, **14-19**.

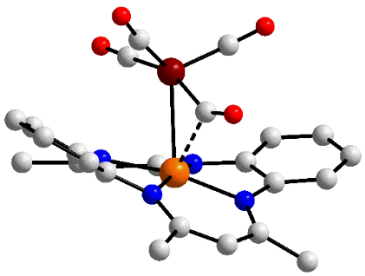

Figure 5. The molecular structure of **18**, highlighting the presence of a semi-bridging CO ligand (dashed line). Additional colour code: cobalt, brown.

The preparation of homo- and hetero-nuclear dimetallic DBTAA complexes based on rhodium and iridium have been described by Fandos *et al*. [50, 51]. As illustrated in Scheme 7, complexes **20a-b** were isolated in good yields when **2a** stirred in the presence of the corresponding dimeric $[Rh(COD)(OH)]_2$ and $[Ir(COD)(OH)]_2$ precursors in toluene at room

temperature [50]. In the same solvent, the mild heating of **20a-b** at 85 ºC with additional (1 equiv.) $[Rh(COD)(OH)]_2$ and $[Ir(COD)(OH)]_2$ afforded the corresponding dicyclooctadiene di-nuclear complexes **21a-b** in good yields. Moreover, ligand substitution was accomplished in **20b** by replacing 1,5-cyclooctadiene (COD) with two CO ligands in a CO atmosphere to furnish the desired complex **22** in 66% yield. This was then reacted with $[Ir(COD)(OH)]_2$ in toluene at 70 ºC to produce a dimetallic complex **23** in 73% yield. The subsequent displacement of cyclooctadiene with two CO ligands afforded the highly hygroscopic tetracarbonyl complex **24** in good yield. The oxidative addition reactions between **24** and several oxidizing agents such as iodine, methyl iodide, diphenyl disulphide and dipyridyl disulphide in dichloromethane at room temperature produced the corresponding products **25a-d** in good yields. The structural features of **24** and **25a** were ambiguously confirmed by crystallographic analysis (Figure 6). The two iridium(I) ions of **24** each adopt a square-planar geometry based on C_2N_2 donor sets (Figure 6a) with a U-shape molecule as the iridium lie above and to the same side of the N_4 plane. Oxidation with iodine yields **25a**, where the addition of iodide leads to a square-pyramidal geometry with the iodide atom occupying the apical position (Figure 6b). The Ir−Ir bond length in **25a**, i.e. 2.772(1) Å, is shorter than the Ir···Ir separation of 3.064(1) Å in **24**. These results are related to the loss of a pair of electrons from the two anti-bonding orbitals of d^8-d^8 in **24** to d^7-d^7 in **25** [51].

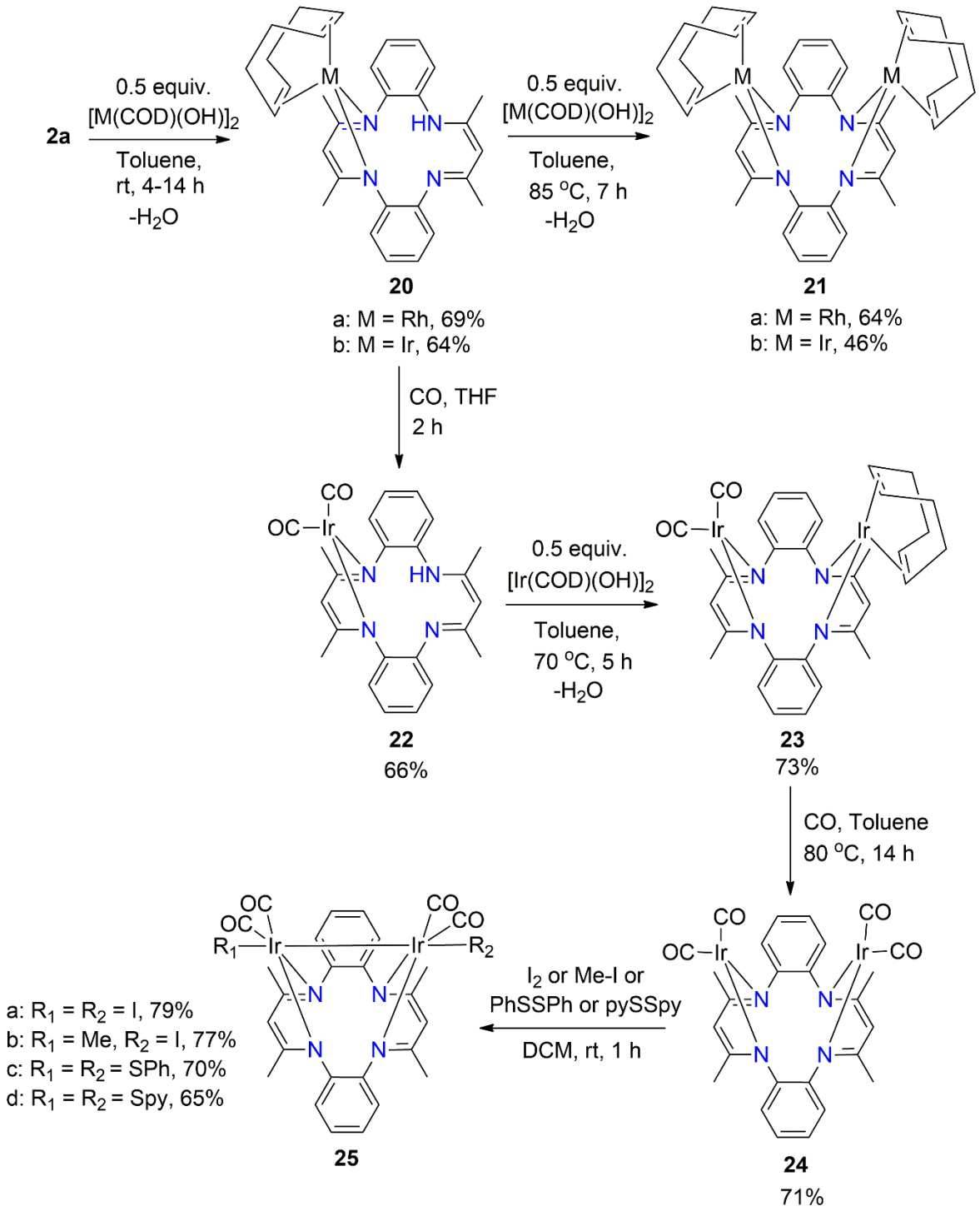

Scheme 7. Synthesis of rhodium(I) and iridium(I/II) DBTAA complexes, **20**-**25**.

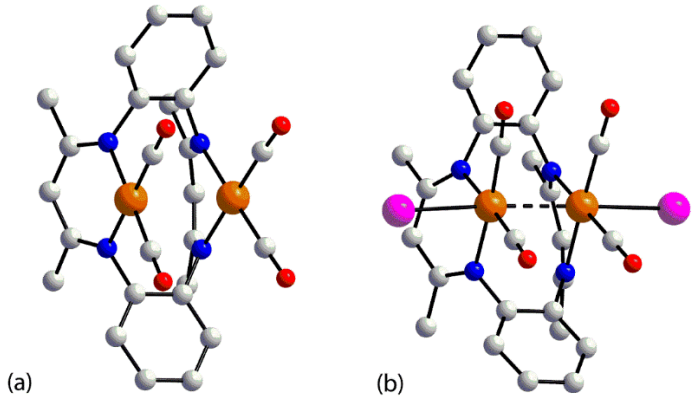

Figure 6. Molecular structures of (a) U-shaped **24** and (b) oxidation product **25a**. The dashed line in (b) represents an Ir···Ir bond [2.7716(2) Å]. Additional colour code: iodide, pink.

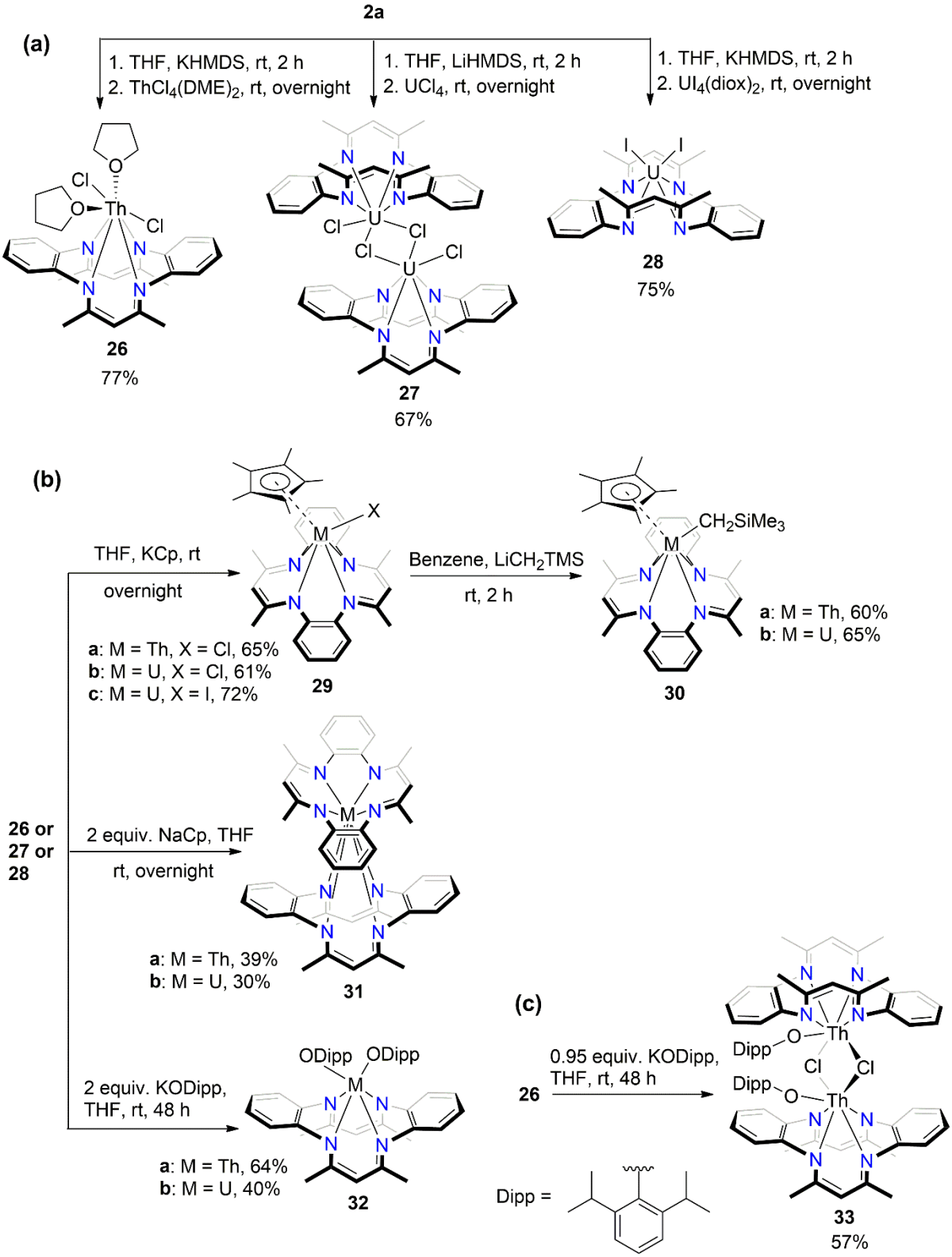

Scheme 8. Synthesis of thorium(IV) and uranium(IV) DBTAA complexes, **26-33**.

Some coordination chemistry of thorium and uranium with DBTAA ligand was reported by Arnold *et al*. [52]. As depicted in Scheme 8a, the di-anionic salt derived from **2a** was generated by the addition of KHMDS or LiHMDS [53] into a solution of **2a** in THF. Subsequently, the addition of one equivalent of $ThCl_4(DME)_2$ [54], UCl_4 [55] or $UI_4(diox)_2$ [56] solutions at room temperature afforded **26-28** in good yields. As illustrated in Figure 7, the molecular structure of **28** adopts an inverse saddle-shaped conformation due to steric congestion between iodide ligands and phenyl rings. Interestingly, the ^{1}H NMR spectrum shows that the two methine protons of **28** appear as a singlet at δ -82.2 ppm due to the strong paramagnetism of the U(IV) centre. This signal is shifted to the upfield region by 94.4 ppm compared to the related nuclei of dimeric **27** [52].

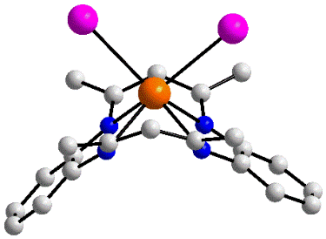

Figure 7. The molecular structure of **28** highlighting the inverse saddle-shaped conformation of DBTAA; the molecule has mirror symmetry.

Next, the preparation of the complexes **29a-c** was achieved by treating the **26-28** precursors with potassium pentamethylcyclopentadienyl (KCp*) with stirring in THF (Scheme 8b). As confirmed by X-ray crystallography, the three complexes exhibit similar geometric features including an inverse saddle-shaped conformation despite the presence of different metal ions and halides. ^{1}H NMR spectroscopy revealed two asymmetric methine signals for **29a** resonating at δ 5.1 ppm {is there a value missing?}, at δ -30.4 and 62.6 ppm for **29b**, and at δ -36.7 and 69.4 ppm for **29c**. The synthetic scope was extended by reacting **29a-b** with $LiCH_2TMS$ in benzene at room temperature to furnish **30a-b** in good yields. Notably, the two methine protons of **30b** shift to the downfield region at δ -6.1 and 39.2 ppm relative to **29b**, whereas the two methine protons of **30a** are not significantly different when compared to **29a** [52].

The sandwich complexes **31a-b** were prepared by reacting **26** and **27** with two equivalents of NaCp in THF at room temperature (Scheme 8b). Interestingly, the complexes **31a-b** can be synthesized directly from the reaction between the di-anionic salt **2a** (2 equiv.) and $ThCl_4(DME)_2$ or UCl_4 (1 equiv.) in THF [57]. The thorium(IV) and uranium(IV) atoms possess near to cubic coordination geometries as described above for **10b** (Figure 4). The UV-vis absorption spectrum of **31b** shows a broad absorption profile between 270 and 670 nm, which is attributed to the π-π* ligand and metal to ligand charge transfer (MLCT) transitions. The electrochemical properties report that **31b** has two distinct and reversible oxidations at -0.73 V and 0.21 V, relative to the ferrocene/ferrocenium. Both peaks are assigned to the uranium(IV/V) and uranium(V/VI) redox couples, respectively [57].

The reactions of **26** and **27** with two equivalents of KODipp in THF solution afforded the corresponding **32a-b** in 64 and 40% yields, respectively. Interestingly, it was found that the reaction of **26** with 0.95 equivalent of KODipp gave a dimeric **33** in 57% yield (Scheme 8c). As verified by X-ray crystallographic analysis, the ODipp ligands in **33** are mutually cis within a highly distorted octahedral N_4O_2 geometry [52].

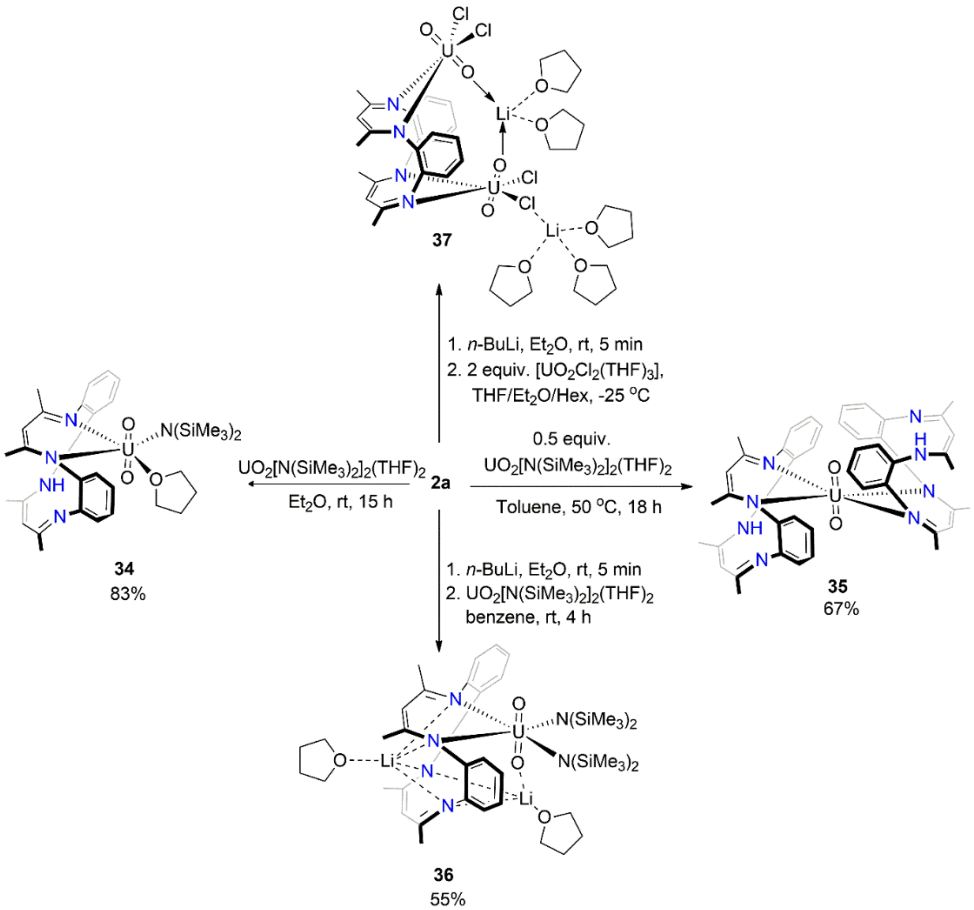

Scheme 9. Synthesis of uranium(VI) DBTAA complexes, **34-37**.

Some coordination chemistry of the uranyl di-cation, $[UO_2]^{2+}$ towards the DBTAA ligand was reported by Hayton *et al*. [58]. The reaction of **2a** with an equimolar amount of $UO_2[N(SiMe_3)_2]_2(THF)_2$ [59] in diethyl ether at room temperature afforded the crystalline solid **34** in excellent yield (Scheme 9) [58]. As seen from Figure 8a, the coordination environment of the uranium(VI) ion in this complex comprises two axial oxido groups, two nitrogen atoms from the propanediiminato fragment of DBTAA, a trimethylsilyl amide-N and a THF-O atom. The resulting coordination geometry is based on an octahedron. It is noted there is a free N−H group in the complex; this forms an intramolecular N−H···N hydrogen bond with the non-coordinating ring-nitrogen atom. Complex **35** was synthesized by the mild heating of a reaction mixture of **2a** (2 equiv.) and $UO_2[N(SiMe_3)_2]_2(THF)_2$ (1 equiv.) in toluene. The uranium centre in **35** exhibits a trans-N_4O_2 donor set within an octahedral geometry. In each of **34** and **35**, the macrocyclic ligands adopt an inverse saddle-shaped conformation.

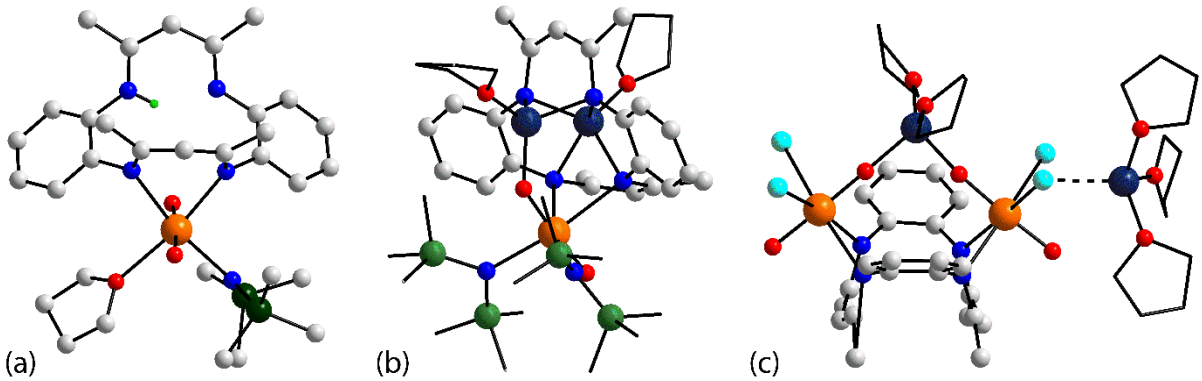

Figure 8. Molecular structures of (a) **34**, (b) **36** (the molecule has mirror symmetry) and (c) **37**. Additional colour code: chloride, cyan; silicon, dark-green; lithium, dark-teal; hydrogen, green. The carbon atoms of the THF molecules in (b) and (c), and the methyl groups of the Me_3Si residues in (b) have been represented in stick form for clarity.

Complex **36** includes the presence of two lithium cations which considerably influences the coordination behaviour of the complex. The di-anionic lithium salt of **2a** was prepared by the reaction of **2a** with *n*-BuLi in diethyl ether at room temperature [60]. The reaction of this salt with an equivalent amount of $[UO_2(N(SiMe_3)_2)_2(THF)_2]$ {should the N-ligand be given as HMDS?} in benzene at room temperature for several hours produced **36** in 55% yield (Scheme 9). The molecular structure of **36** was established by X-ray crystallography (Figure 8b); the

molecule is bisected by a mirror plane consisting of the metal ions. One Li^+ centre interacts with four nitrogen atoms of the macrocycle moiety, ensuring a folded conformation, and a THF molecule, whereas the second Li^+ cation interacts with two nitrogen atoms of the macrocycle, an oxido atom as well as a second THF molecule [58]; the donor set for uranium is trans-N_4O_2.

Further experimental work reported that the addition of $[UO_2Cl_2(THF)_3]$ [61] (2 equiv.) into a solution of the lithium salt of **2a** (1 equiv.) at -25 ºC gave a mixture of complex **37** and an unidentified product in 44% yield (Scheme 9), in the ratio of 5:1, as suggested by ^{1}H NMR spectroscopy. However, the purification of the unknown species was not possible owing to the instability. The X-ray crystal structure of **37** (Figure 8c) shows a $[Li(THF)_2]^+$ cation sits atop of the complex molecule being connected via two Li···O(oxido) interactions, whereas the $[Li(THF)_3]^+$ ion interacts with a chlorido ligand. The DBTAA ligand bridges two $[UO_2Cl_2]$ centres, chelating each uranium atom via two nitrogen atoms; the $Cl_2N_2O_2$ donor set defines a distorted octahedral geometry in each case [60].

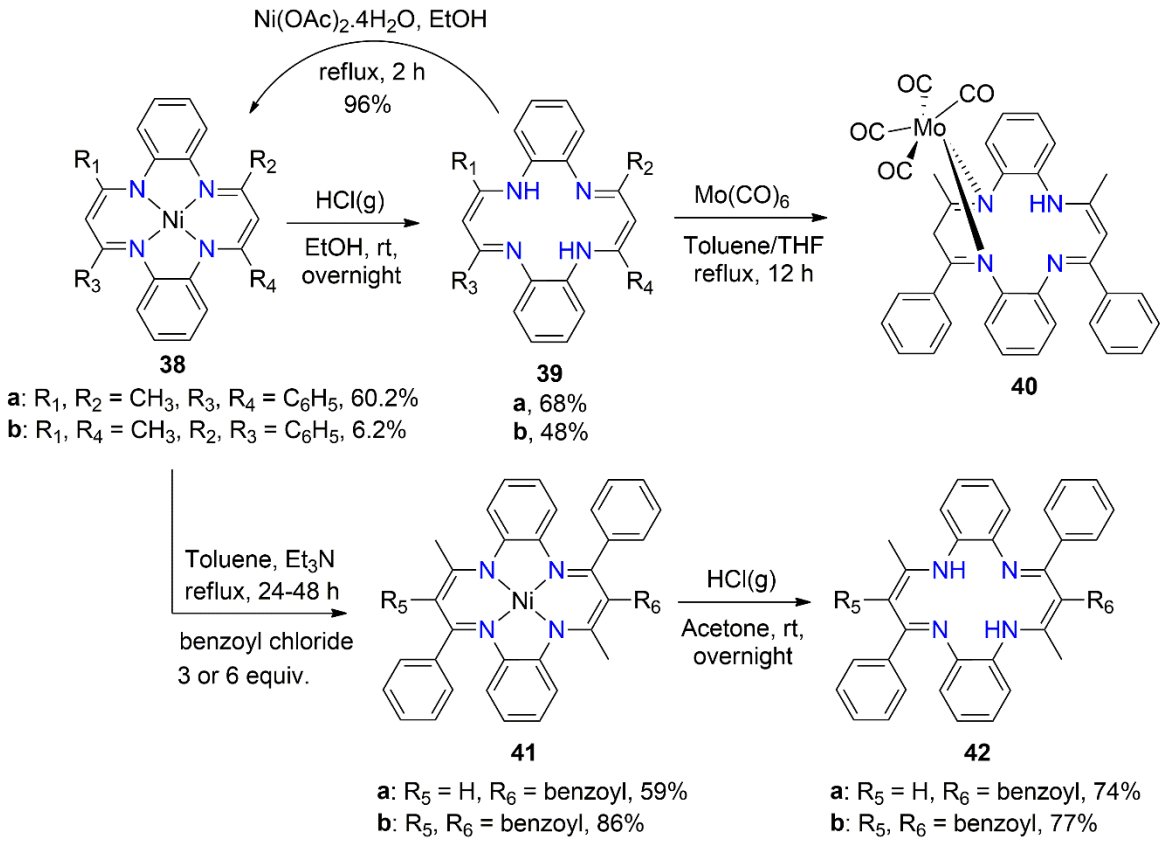

Scheme 10. Synthesis and core-functionalization of DBTAAs, **38-42**.

A versatile synthetic protocol to functionalize the DBTAA core was reported by Shen *et al*. [33]. Referring to Scheme 10, the template reaction between *o*-phenylenediamine and 1-benzoylacetone in the presence of nickel(II) in refluxing ethanol produced a mixture of isomers **38a-b** in 66.4% yield. To separate the isomers, the crude product was washed with *n*-butyl alcohol, leaving crude **38a**, which was later recrystallized to obtain a pure crystalline product in 59% yield. Crude **38b** containing small amounts of **38a** was isolated in 7.4% yield, in the ratio of 1:5, which is inseparable by chromatographic and crystallization methods. Therefore, the total ratio of **38a** and **38b** is assumed to be 10:1. Next, the demetalation of pure **38a** and crude **38b** led to the formation of pure **39a-b** in good yields**.** Complex **38b** was obtained in 96% yield when ligand **39b** was subjected to the reaction of $Ni(OAc)_2.4H_2O$ in refluxing ethanol [33].

The heating of an equimolar amount of **39a** with $Mo(CO)_6$ in toluene produced complex **40** (Scheme 10). Notably, X-ray crystallography revealed one methine carbon to be protonated by the migration of the N−H proton upon coordination to the $Mo(CO)_4$ moiety (Figure 9). The distorted octahedral environment of the molybdenum(0) comprises two nitrogen atoms of the imino-propane fragment and four carbonyl ligands. A computational analyses proved the importance of short intramolecular $\sigma \rightarrow \pi^*$ (C–H···CO) and C–H··· interaction in stabilizing the twisted conformation of the bidentate ligand [62].

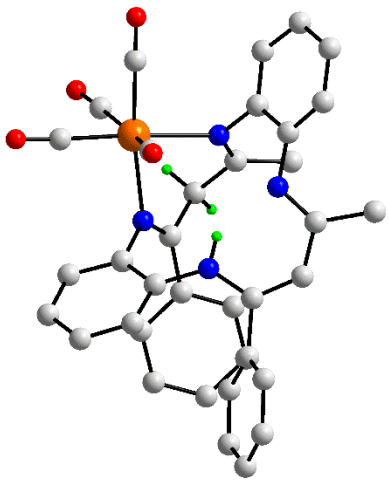

Figure 9. The molecular structures of **40** highlighting the presence of the methylene link within the DBTAA derivative.

Following this work, Shen *et al*. [63] functionalized the *meso*-position of complex **38b** by substituting the benzoyl group. Complexes **41a-b** were prepared in good yields by treating **38b** with three and six equivalents of benzoyl chloride, respectively, in the presence of

triethylamine under refluxing conditions. This proved to be a powerful tool for the introduction of various substituents into the macrocyclic core in the absence of a metal catalyst. Later, a classical demetallation protocol was utilized to generate **42a-b** in good yields (Scheme 10) [63].

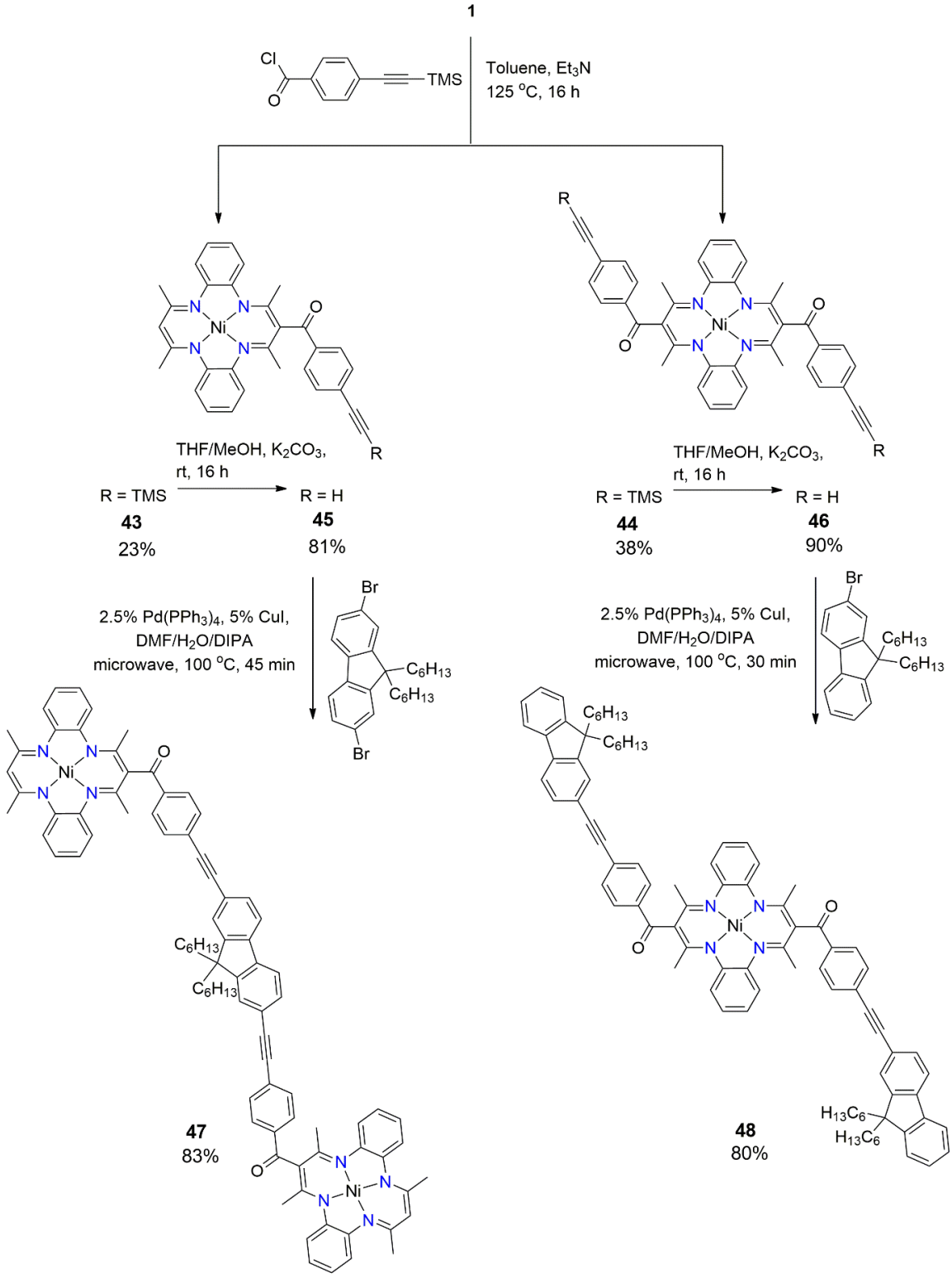

Scheme 11. Synthesis of extended π-conjugation of nickel(II) DBTAA complexes, **47**-**48**.

The functionalization of the macrocyclic core was also reported by Gilroy *et al*. [64]. Compounds **43** and **44** were obtained by the treatment of **1** with 4-((trimethylsilyl)ethynyl) benzoyl chloride in the presence of triethylamine (Scheme 11). The removal of the TMS leaving group was achieved under basic conditions to afford the intermediates **45** and **46** in 81 and 90% yields, respectively. The subsequent Sonogashira coupling-reaction between **45** and 2,7-dibromo-9,9-dihexyl-9*H*-fluorene proceeded smoothly under microwave irradiation to furnish binuclear **47** in 83% yield. In a similar manner, **48** was formed rapidly in 80% yield when **46** was subjected to 2-bromo-9,9-dihexyl-9*H*-fluorene (Scheme 11) [64, 65].

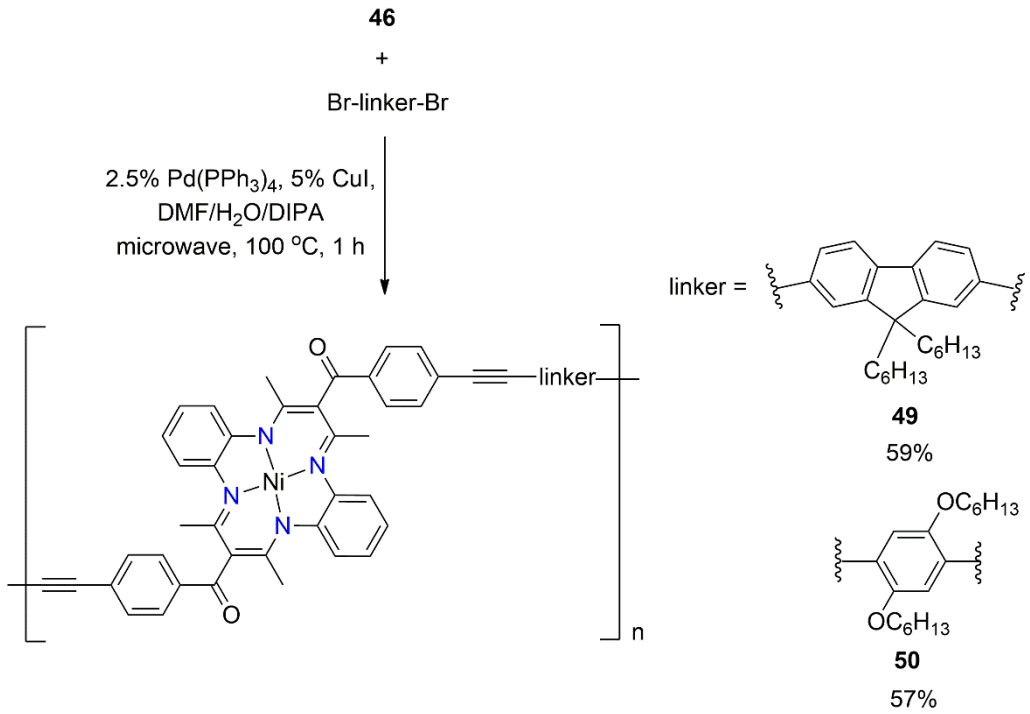

Scheme 12. Synthesis of nickel(II) DBTAA polymers, **49** and **50**.

In related chemistry synthesis, the Sonogashira reaction effectively coupled the monomer **46** with 2,7-dibromo-9,9-dihexyl-9*H*-fluorene or 1,4-dibromo-2,5-bis(hexyloxy)benzene linkers to obtain polymers **49** and **50**, respectively, in good yields (Scheme 12). The absorption spectrum of **49** displays two intense peaks at 275 and 378 nm, which correspond to the π-π* transitions of the macrocyclic core and the benzoyl-linked fluorene, respectively. A smaller peak at 588 nm is assigned to the LMCT. It was found that the absorption parameters of polymer **50** are almost the same as those for **49**, but that the second absorption peak exhibits a red-shift by 9 nm due to the extension of the π-conjugation linkage between the benzoyl and phenyl linkers. Gel Permeation Chromatography (GPC) analysis of **49** and **50** gives (M_n = 7825 g mol^{-1}, M_w = 11800 gmol^{-1}, $Đ$ = 1.51) and (M_n = 6675 g mol^{-1}, M_w = 18250 g mol^{-1}, $Đ$ = 2.77), respectively. The comparative value of $Đ$ indicates that the polymer **50** has a broad molecular weight distribution compared to that of polymer **49**. Interestingly, both polymers exhibit almost similar electrochemical properties, where two reversible one-electron oxidation potentials are detected around 0.24 and 0.75 V, relative to the ferrocene/ferrocenium redox couple [64, 65].

Another versatile synthetic pathway for the preparation of the polymers containing DBTAA analogues was investigated by Luh *et al*. [66]. As outlined in Scheme 13, the benzoylation reactions of **1** or **2a** with excess 4-bromobenzoyl chloride gave rise to **51a-b** in moderate yields. To extend the synthetic scope, **51b** was converted into the corresponding **51c** by a metalation reaction. In particular, the Sonogashira cross-coupling reaction of **51a** with an alkyne precursor **52** in the presence of $Pd(PPh_3)_4$, CuI and piperidine furnished the monomer **53a** in 65% yield. To obtain monomers **53b-c**, $Pd(PPh_3)_2Cl_2$ was used as the catalyst in the coupling reaction between **51b-c** and **52** in refluxing piperidine. Polymers **54a-c** were prepared in excellent yields via the ring-opening metathesis polymerization (ROMP) reaction of the monomers **53a-c** in the presence of Grubbs I catalyst in dichloromethane. This reaction occurs smoothly under facile conditions without the tedious purification of the product. The UV-vis absorption spectra reveal that the metal-to-ligand charge-transfer (MLCT) peak for **54a** and **54c** is located at 392 and 414 nm, respectively, while the LMCT peak is observed at 588 and 501 nm, respectively. GPC analysis yields **54a** (M_n = 9509 g mol^{-1}, M_w = 11950 gmol^{-1}, $Đ$ = 1.26), **54b** (M_n = 9709 g mol^{-1}, M_w = 11990 gmol^{-1}, $Đ$ = 1.23) and **54c** (M_n = 13818 g mol^{-1}, M_w = 16900 gmol^{-1}, $Đ$ = 1.22), indicating that the polymerization protocol gives a consistent $Đ$ value regardless of the substituent effect on the N_4 core. Furthermore, the electrochemical

properties of the metal-containing polymers **54a** and **54c** display a reversible first oxidation potential at 0.24 and 0.21 V, whereas metal-free polymer **54b** shows an irreversible first oxidation potential at 0.48 V [66].

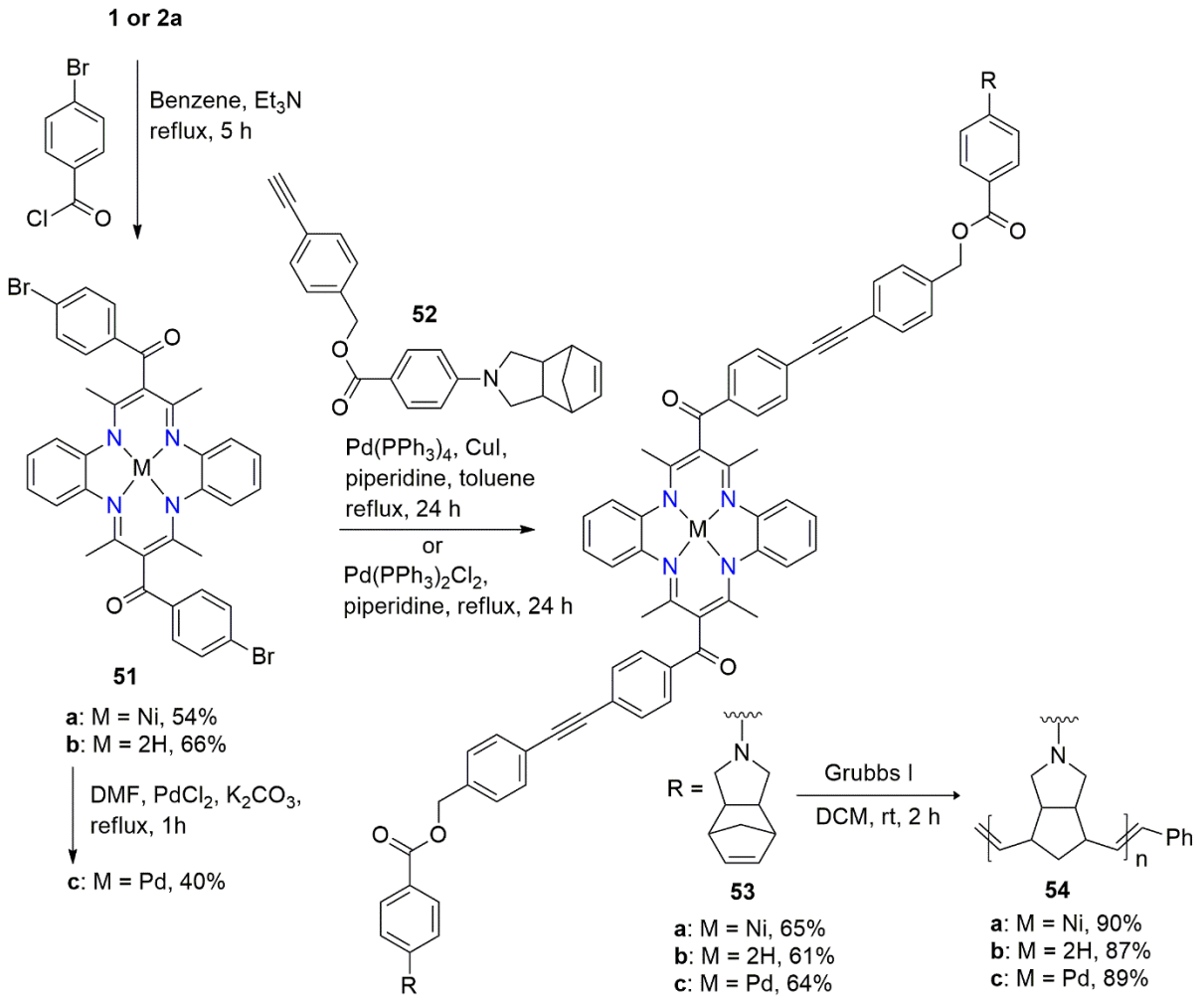

Scheme 13. Synthesis of DBTAA polymers, **54a-c**.

The following methodology was described by Gilroy *et al*. in 2017 [67]. As shown in Scheme 14, the preparation of an asymmetric intermediate **57** was synthesized in a manner similar to a literature procedure [65]. A 'click' reaction between the **57** and an azide precursor forms the monomer **58** in moderate yield. In the final step, the ROMP reaction of the monomer with Grubbs III catalyst successfully produced polymer **59** in a high conversion yield. The spectroscopic studies reported that both the monomer and polymer have a similar absorption pattern, where the π-π* and LMCT transition peaks are clearly observed at 390 and 590 nm, respectively. GPC analysis shows that polymer **59** has a narrow molecular weight distribution

with M_n = 24100 g mol^{-1}, M_w = 26500 g mol^{-1} and $Đ$ = 1.12. The cyclic voltammetry analysis indicates that the polymer has two reversible one-electron oxidation potentials at 0.21 and 0.70 V. A reversible one-electron reduction potential is also detected at -2.07 V [67]. Although progress has been achieved in the synthesis of the polymer-based DBTAA in recent years, no specific application has been investigated, however. The synthetic pathway for the preparation of DBTAA-based polymer offers several advantages such as facile methodology, high conversion yields and well tolerated on functionalized terminal alkynes.

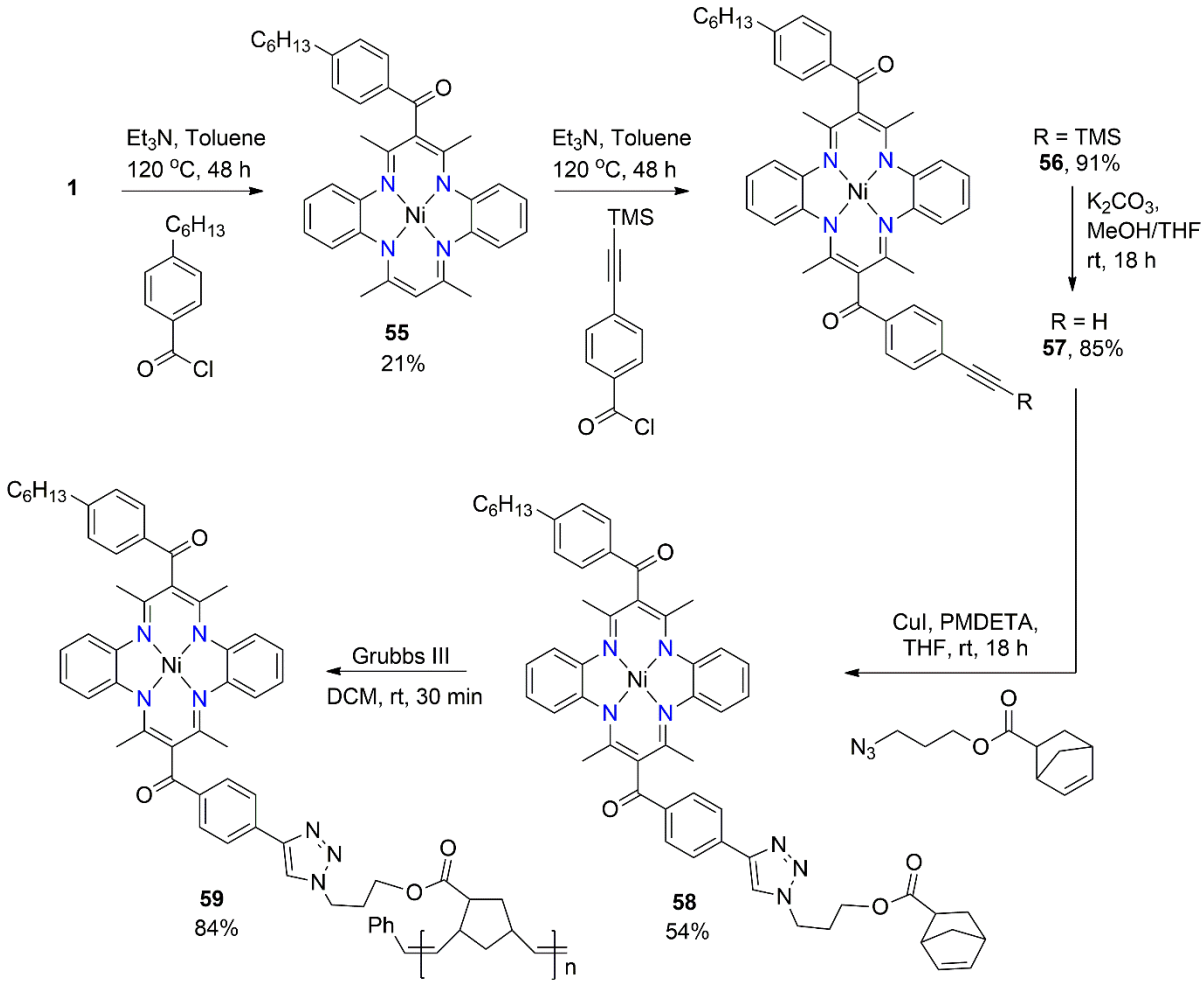

Scheme 14. Synthesis of Ni(II) DBTAA polymer **59**.

5. Synthesis and reactivity of *meso*-pyridyl DBTAA

Pyridyl *meso*-substituted DBTAA, **H₂60** (Scheme 15) was first synthesized by Reichardt and Scheibelein [68] in 1978 through a non-template condensation reaction between

2-(4-pyridinyl)malonaldehyde and *o*-phenylenediamine in the presence of a catalytic amount of acetic acid in refluxing ethanol [68, 69].

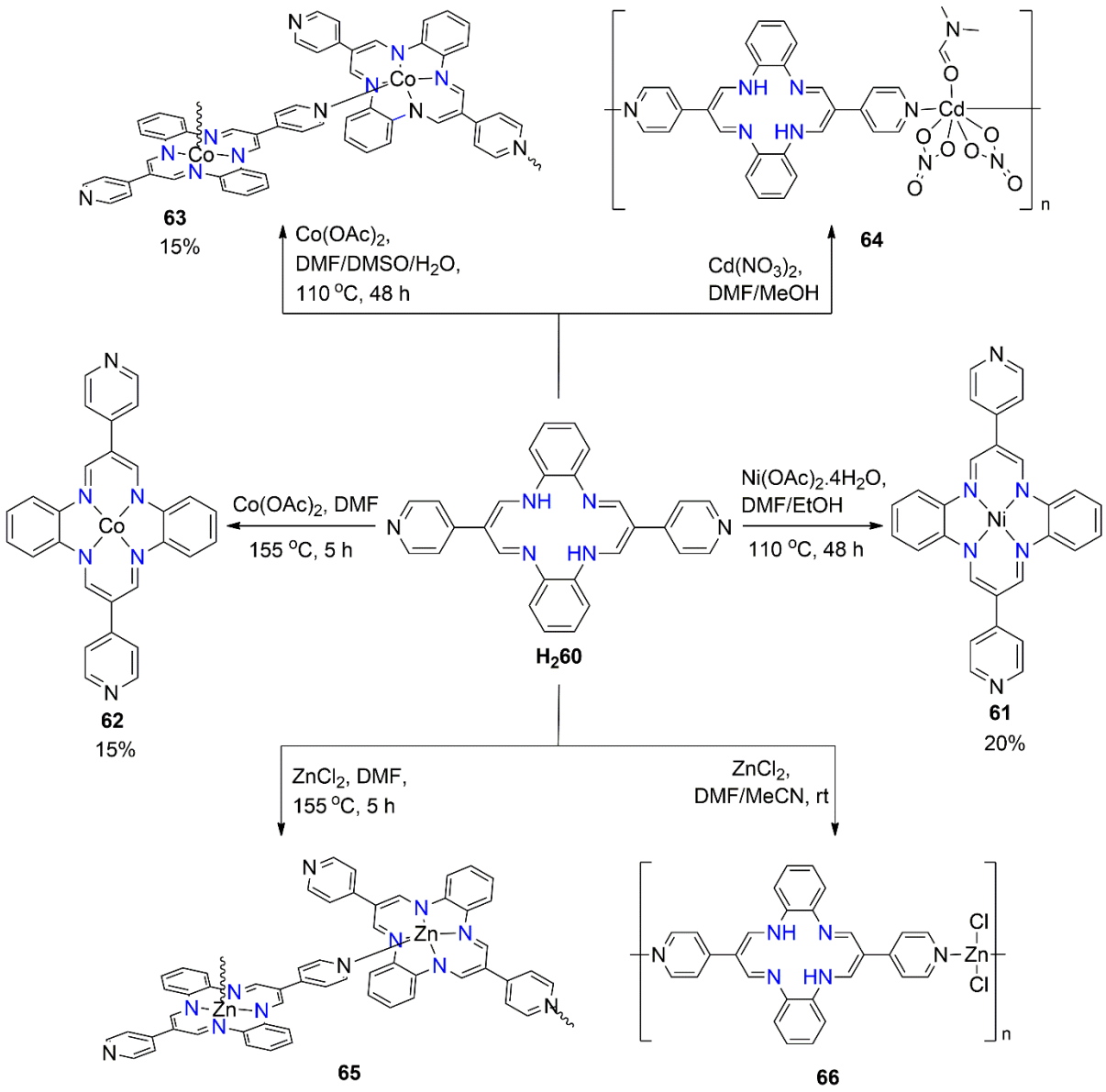

Scheme 15. Synthesis of pyridyl *meso*-substituted DBTAA complexes, **61**-**66**.

The simplest structure, i.e. **61**, was prepared by the metalation of **$H_2$60** with $Ni(OAc)_2.4H_2O$ under mild heating (Scheme 15). Refluxing **$H_2$60** with cobalt(II) acetate in DMF led to the formation of **62** in poor yield. Interestingly, the replacement of DMF with a solvent mixture comprising DMF, DMSO and H_2O, in the ratio 6:1:2, produced **63** in 15% yield. This indicates that the solvent system plays an important role in the production of the complexes. X-ray crystallography on **63** reveals the presence of a coordination polymer (Figure 10a). The cobalt(II) atom is tetra-coordinated within the ring cavity and extends its

coordination number to five with a square-pyramidal geometry by connecting to a pyridyl-nitrogen atom of a symmetry related molecule to generate a one-dimensional helical chain [70]. Treatment of **$H_2$60** with an excess of $Cd(NO_3)_2$ resulted in the formation of **64**. Structural analysis shows that the cadmium(II) atom is not coordinated within the ring, rather is exocyclic, being bridged by two pyridyl-nitrogen atoms of **$H_2$60** derived from two symmetry related molecules (Figure 10b). The pentagonal-bipyramidal geometry is completed by two chelating nitrate anions and a DMF molecule; the pyridyl-nitrogen atoms occupy the axial positions with the resulting one-dimensional chain having a zig-zag topology. The metalation reaction between **$H_2$60** and $ZnCl_2$ in refluxing DMF afforded complex **65**. The polymeric chain of **65** is isostructural to **63**. The preparation of complex **66** was achieved smoothly by stirring **$H_2$60** with $ZnCl_2$ in DMF and MeCN media. X-ray crystallography of **66** shows that the $ZnCl_2$ moiety is coordinated by two bridging pyridyl-nitrogen atoms leading to a distorted tetrahedral geometry for zinc, within a Cl_2N_2 donor set (Figure 10c). The topology of the chain is helical [71].

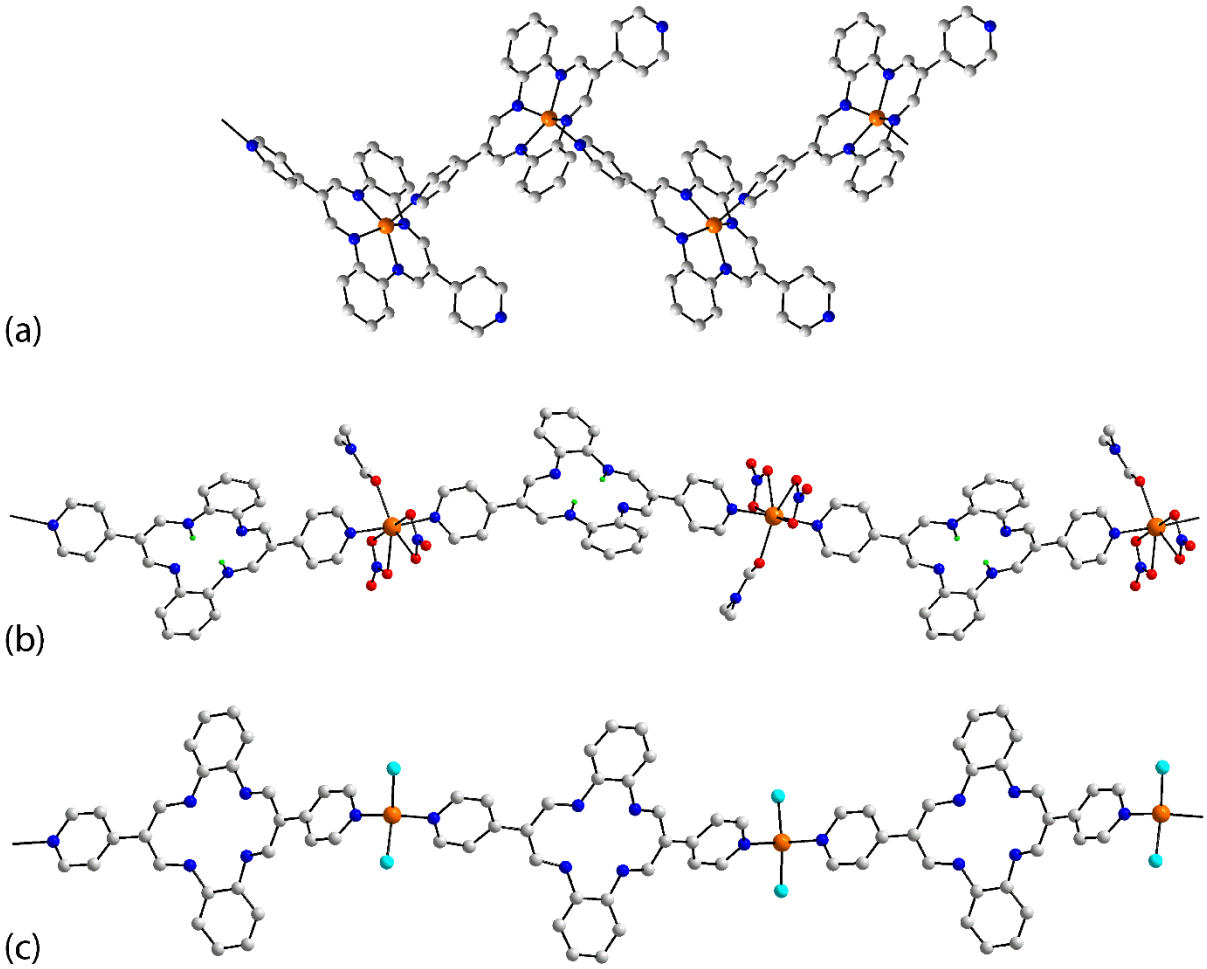

Figure 10. Views of the one-dimensional coordination polymers in the crystals of (a) **63**, (b) **64** and (c) **66** (the nitrogen-bound hydrogen atoms of the ring were not located in the analysis).

Referring to Scheme 16, a one-pot, three component reaction of **$H_2$60**, $Zn(NO_3)_2.4H_2O$ and isophthalic acid (H_2PA) in the presence of hydrochloric acid afforded a two-dimensional coordination polymer, **67**. X-ray crystallography shows that the zinc(II) centre is out of the N_4 plane, being coordinated by two pyridyl-nitrogen atoms instead. The array comprises undulating rows of $\{Zn(m\text{-isophthalato})_2\}_n$ molecules, with one carboxylate group being asymmetrically chelated and the other in a monodentate mode, cross-linked by molecules of **$H_2$60** (Figure 11) [70].

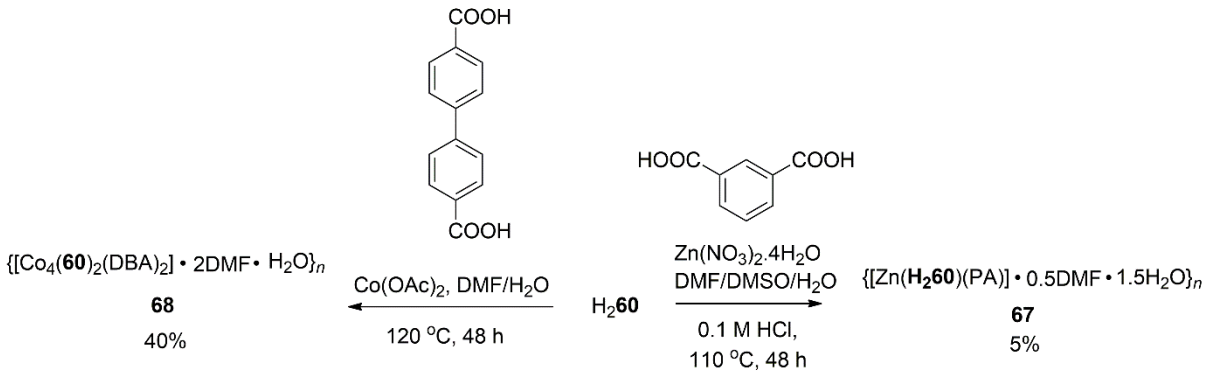

Scheme 16. Synthesis of polymeric DBTAA complexes **67** and **68**.

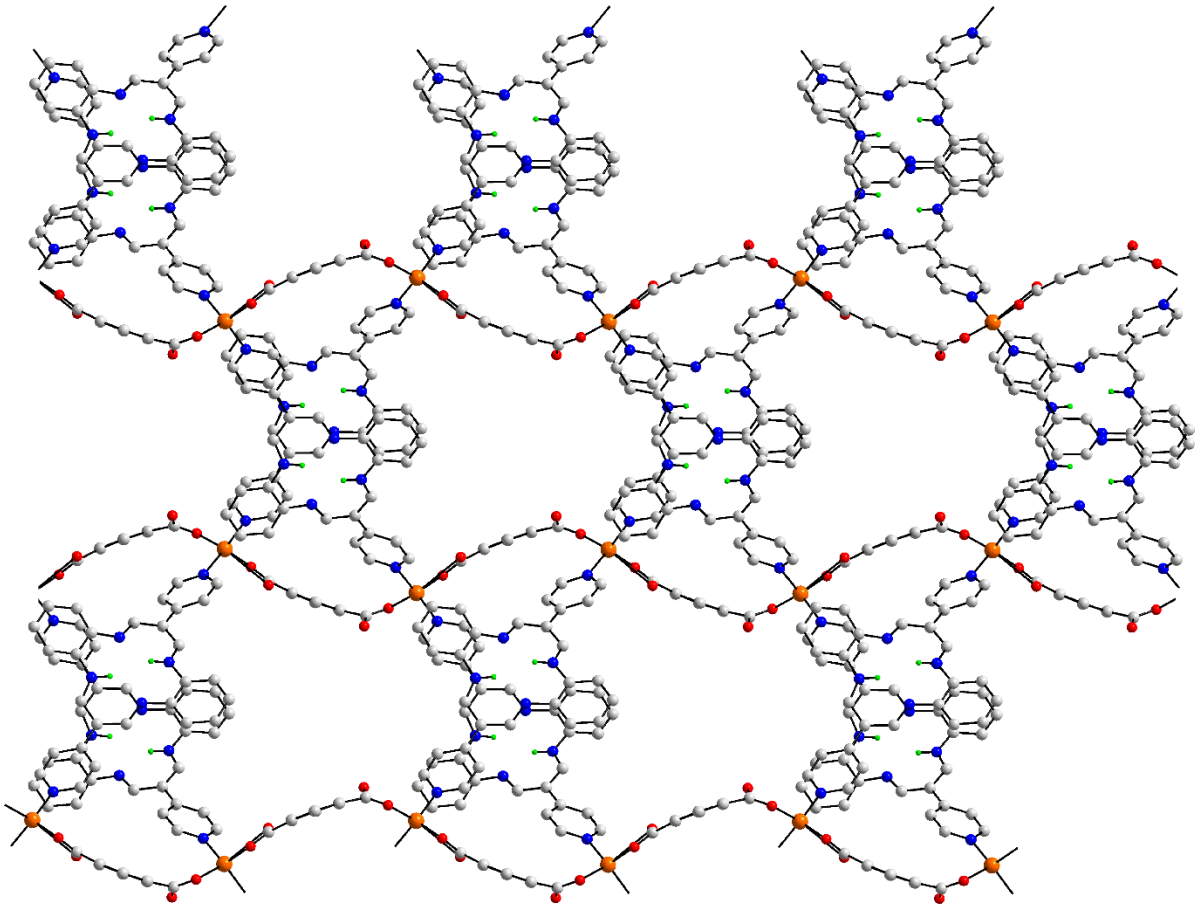

Figure 11. A plan view of the two-dimensional coordination polymer in the crystal of **67**.

A three-dimensional metal organic framework (MOF) is formed in the crystal of **68** which was formed when biphenyl-4,4'-dicarboxylic acid (H_2DBA) was added to a mixture of **$H_2$60** and Co(II) acetate at 120 ºC. In **68**, half the cobalt(II) atoms are coordinated within the cavity while the others are exocyclic; there are two independent biphenyl-4,4'-dicarboxylate di-anions: one functions as a tetradentate ligand, bridging the four cobalt(II) centres while the other functions as a monodentate ligand at each end. No further coordination occurs for the cobalt(II) atoms within the ring but the exocyclic cobalt(II) centres are connected to two pyridyl-N atoms derived from two different DBTAA derivatives, and four oxygen atoms derived from three different dicarboxylate ligands with a three-dimensional architecture (Figure 12). The solid-state photoluminescence spectrum of **$H_2$60** clearly displays a broad emission centre at 655 nm with an excitation peak at 365 nm. However, no emission peaks were observed for **61**, **62** and **68** relative to **$H_2$60** due to the energy loss by non-radiative decay [70].

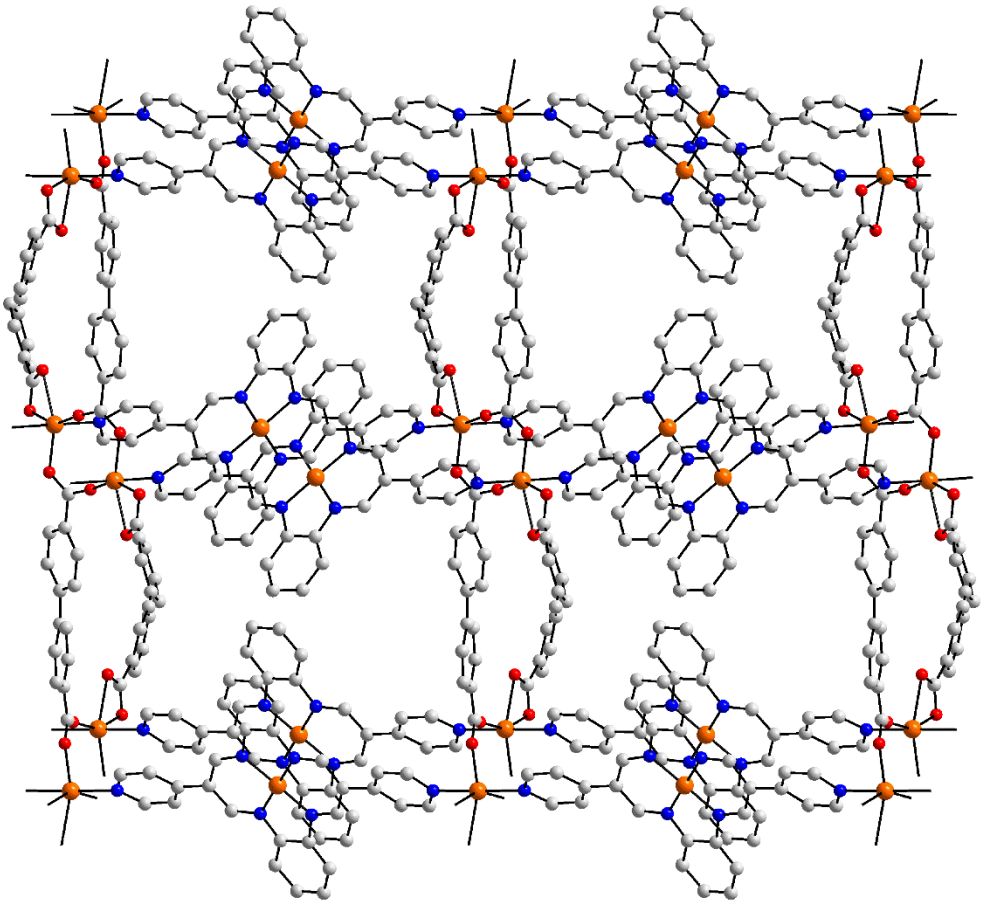

Figure 12. A view of the three-dimensional coordination polymer in the crystal of **68**.

6. Synthesis and reactivity of *meso*-indoleninyl-DBTAA

The *meso*-indoleninyl DBTAA ligand, **69a** (Scheme 17) was first synthesized by Khaledi *et al*. in 2013 from a non-template method employing 2-(diformylmethylidene)-3,3-dimethylindole and *o*-phenylenediamine catalysed by acetic acid in refluxing ethanol Treatment of **69a** with several metal precursors such as $Ni(OAc)_2.4H_2O$, $CoCl_2$ and $CuCl_2$ in the presence of triethylamine afforded the square-planar complexes **70-72** in high yields (Scheme 17) [72]. A similar methodology was also described by Ramle *et al*. [3, 73] who diversified and extended the π-conjugation system of indoleninyl-DBTAA framework (Figure 13).

Interestingly, the magnetic susceptibility measurement of complex **70** demonstrates unusual magnetism properties in the solid-state. The complex is diamagnetic when the temperature is close to 0 K but becomes paramagnetic when the temperature is above 13 K.

This suggests that there is a small energy gap between the LUMO and HOMO, which allows a thermally excited electron to be excited to the triplet state [74]. Furthermore, computational calculations were also performed to study the magnetism of **70** [75]. The solid-state UV-vis spectrum indicates that compound **69a** has a strong absorption profile between 200 and 600 nm. In comparison, the spectra of **70-72** show a red-shift due to the tuning of the π-π* transitions within the macrocyclic ligand and charge-transfer (CT) transitions from metal to ligand [72, 76]. In a dilute chloroform solution, the UV-vis absorption spectrum of **69a** has a maximum peak at 377 nm, which is attributed to the π-π* transition of the molecule [75]. This peak is red-shifted to 395 nm in the presence of octyloxyl-alkyl chains in **69b**. Compared to **69b**, the absorption peak of **69c** shows a red-shift to 417 nm when the π-conjugation system on the indolenine moiety is extended [73].

Referring to Figure 13, complexes **70b-c** were utilized as sensitizers in DSSCs with overall efficiencies of 0.036 and 0.093%, respectively. The poor performance of these complexes is due to inefficient charge transfer of the sensitizers from the excited state to the conduction band of TiO_2 [3].

As indicated in Scheme 17, the slow diffusion of $MnBr_2.4H_2O$ or $MnCl_2.2H_2O$ solutions into a dilute solution of **69a** successfully produced the crystals of **73** and **74**, respectively. X-ray crystallography confirms that manganese(II) is oxidized to manganese(III) during the course of reaction. The manganese(III) ions exhibit a square-pyramidal geometry, being coordinated by the tetradentate di-anionic N_4-donor and an apical halide.

The addition of $FeCl_2.4H_2O$ into a solution of **69a** produced a crystalline complex, **75**. It is fascinating that the ligand **69a** undergoes an imine-enamine tautomerism in the presence of a metal salt. As a result, the two nitrogen atoms of the indoleninyl moieties are protonated. As seen from Figure 14a, the oxidized iron(III) ion possesses an octahedral geometry defined by a trans-Cl_2N_4 donor set. One of the protonated indoleninyl groups interacts with a chloride anion, via a N–H···Cl hydrogen bond, so the complex is isolated in neutral form. The binuclear complex **76** was synthesized in good yield by treating **69a** with $Pd(OAc)_2$ in refluxing THF (Scheme 17). The X-ray crystal structure (Figure 14b) shows that each palladium(II) centre is doubly bridged by two indoleninyl-N atoms and further coordinated by two monodentate acetate anions leading to a square-planar geometry; the two N−H protons remain free in each of the central cavities.

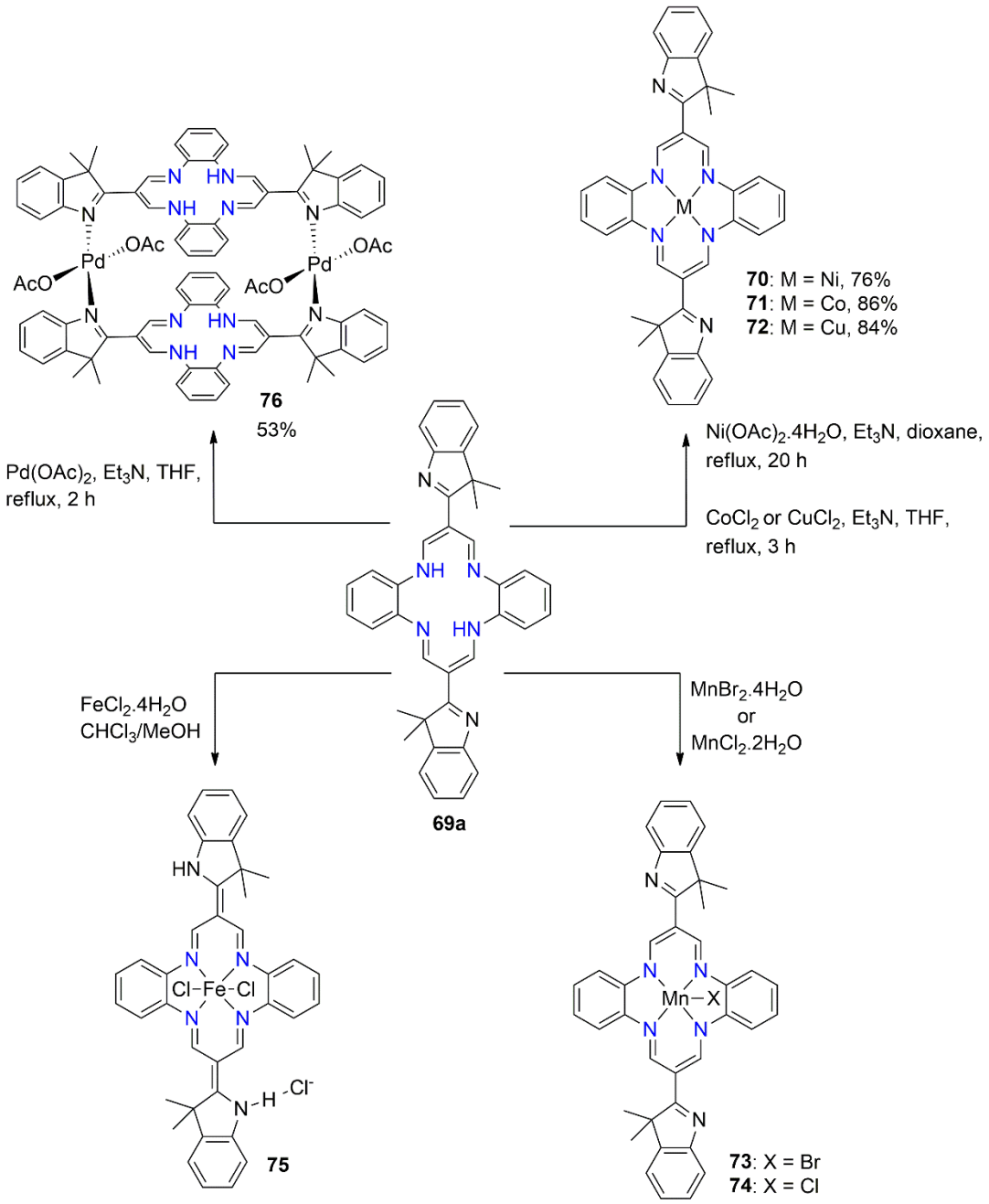

Scheme 17. Synthesis of indoleninyl *meso*-substituted DBTAA complexes, **70-76**.

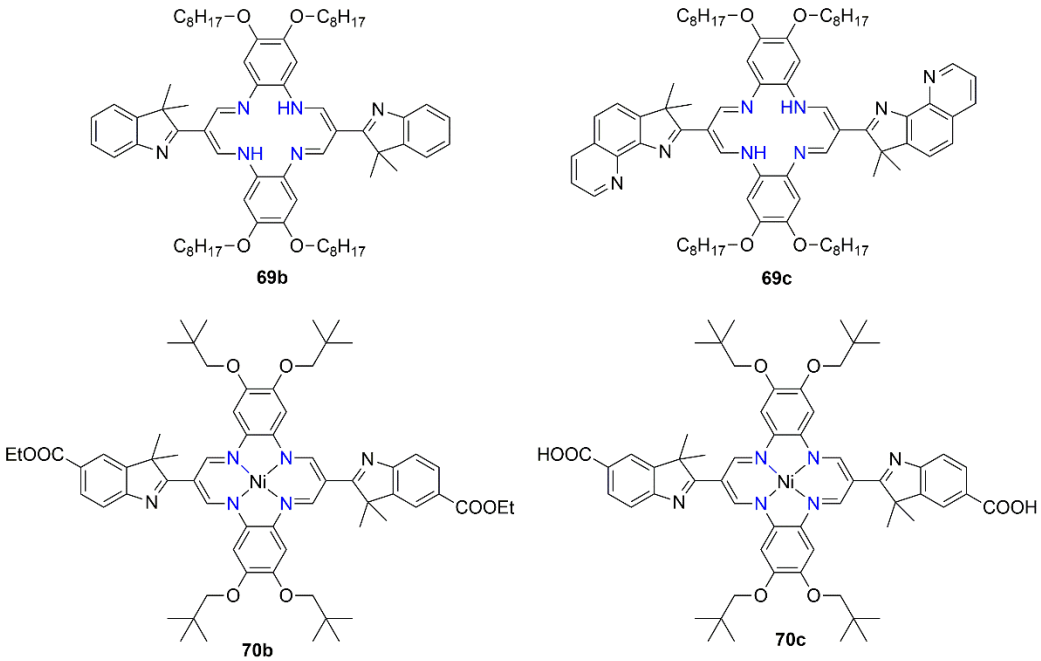

Figure 13. Chemical structures of **69b-c** and **70b-c**.

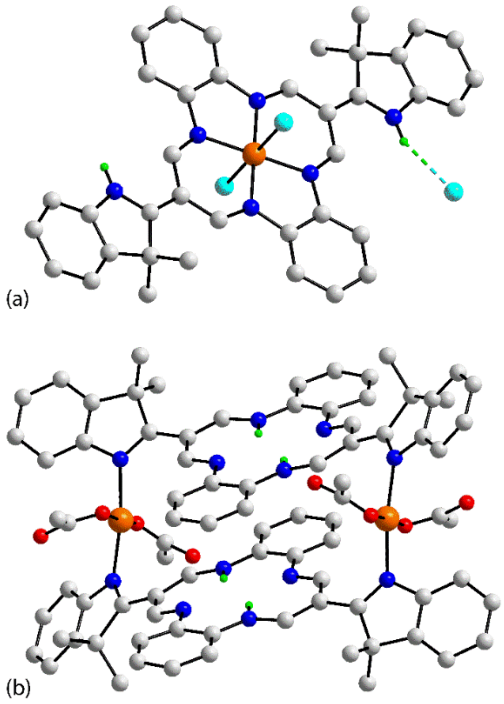

Figure 14. Molecular structures of (a) **75** and (b) **76**. The N–H···Cl hydrogen bond in **75** is shown as a dashed line.

In an effort to further investigate the above chemistry, the preparation of several heterometallic nickel(II)-palladium(II) complexes was accomplished. The reaction was performed by simply stirring a mixture of **70** with an equimolar amount of $Pd(OAc)_2$ in acetic acid at room temperature which afforded two isomers **77** and **78** in 47% yield, in the ratio of 9:1, as suggested by ^{1}H NMR spectroscopy (Scheme 18). The isomers were separated based on their differential solubility in acetone-d_6, with **77** being insoluble in this solvent. The chemical structures for both isomers were well characterized by 1D- and 2D-NMR spectroscopy. X-ray crystallography revealed two, almost parallel units of **70** to be linked, via Pd–N(indoleninyl) bonds. The square-planar geometry for palladium(II) was completed by two monodentate coordinating acetate anions in each case. In **77**, one N_2O_2 donor set possesses a cis-disposition of oxygen atoms while the other possesses a trans-disposition (Figure 15a). In **78**, both square-planar geometries for palladium(II) are trans (Figure 15b). NMR conducted in CD_2Cl_2-d_2 solution showed the slow transformation of **77** into the isomer **78** over several days. Close Ni···Ni contacts are noted in the tetra-nuclear molecules. The Ni···Ni separation in **77** is 3.91 Å while it contracts to 3.22 Å in **78** [77].

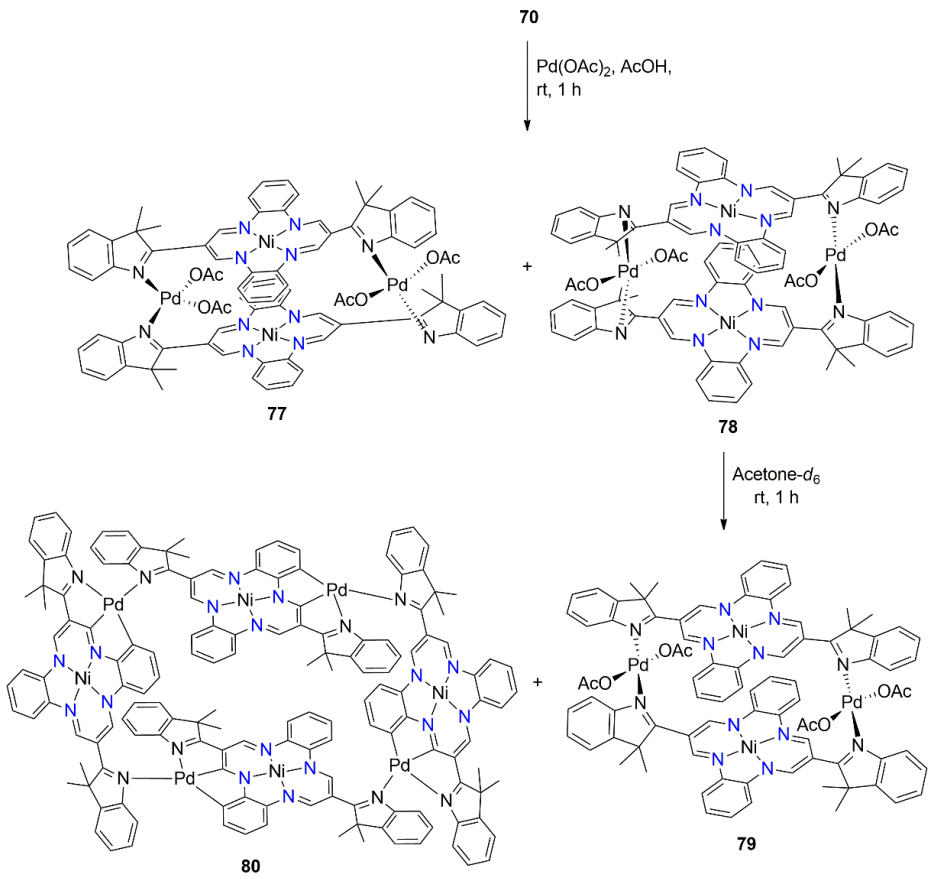

Scheme 18. Synthesis of heterometallic nickel(II)−palladium(II) indoleninyl *meso*-substituted DBTAA complexes, **77**-**80**.

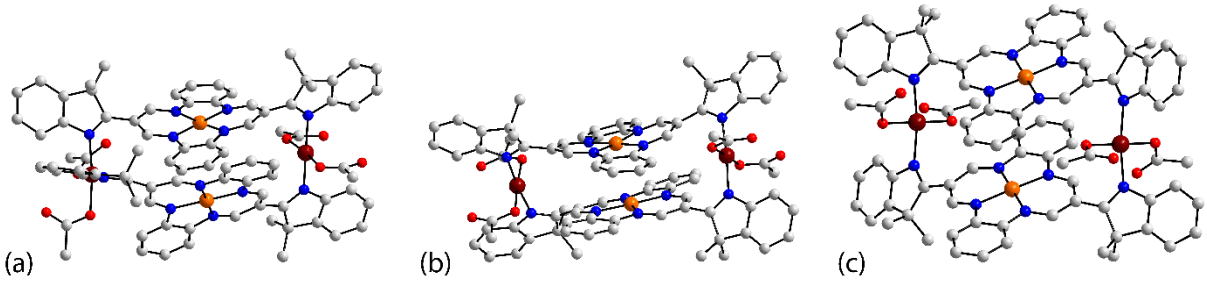

Figure 15. Molecular structures of heterometallic and tetra-nuclear (a) **77**, (b) **78** and (c) **79**. Additional colour code: palladium, brown.

It was also reported that the isomerization of **78** occurred in acetone-d_6 and led to the isolation of crystals readily distinguished by their morphology (Scheme 18). Unambiguous structure determination of **79** and **80** was afforded by X-ray crystallography. The structure of **79** is a conformational isomer of **78**, having trans-N_2O_2 donor sets for palladium(II) (Figure 15c); the molecule is located about a centre of inversion. The conformers largely arise as a result of a rotation about the indoleninyl-C–C(DBTAA) bond, which possess different relative orientations for the PdN_2O_2 square-planes; the transannular Ni···Ni separation in **79** is 5.40 Å. A clear differentiation between the structures of **77-79** rests in the dihedral angles formed between the CO_2 atoms of the carboxylate residues bound to each palladium(II) centre. In **77**, the *cis*-orientated carboxylate residues form a dihedral angle of 83.4° compared to the dihedral angle of 7.2° between the trans-orientated carboxylate residues. In **78**, both dihedral angles, i.e. 6.5 and 7.3°, are indicative of co-planar arrangements. In centrosymmetric **79**, both dihedral angles are 59.5° and are indicative of splayed dispositions [77].

The second decomposition product, **80**, presents a fascinating octa-nuclear cluster comprising of alternating nickel(II) and palladium(II) atoms. While the nickel(II) is coordinated as in **77-79**, an unprecedented mode of bonding is observed for palladium(II). As highlighted in Figure 16, in addition to being coordinated by two cis-orientated indoleninyl-nitrogen atoms derived from two different molecules, the palladium(II) centre is chelated by a doubly-deprotonated DBTAA ligand via the phenyl- and imine-carbon atoms. This phenomenon arises owing to the activation of both β-C–H and phenylene-C–H bonds, in a mechanism involving an electrophilic C–H activation pathway promoted by the acetate anions of the precursor [77].

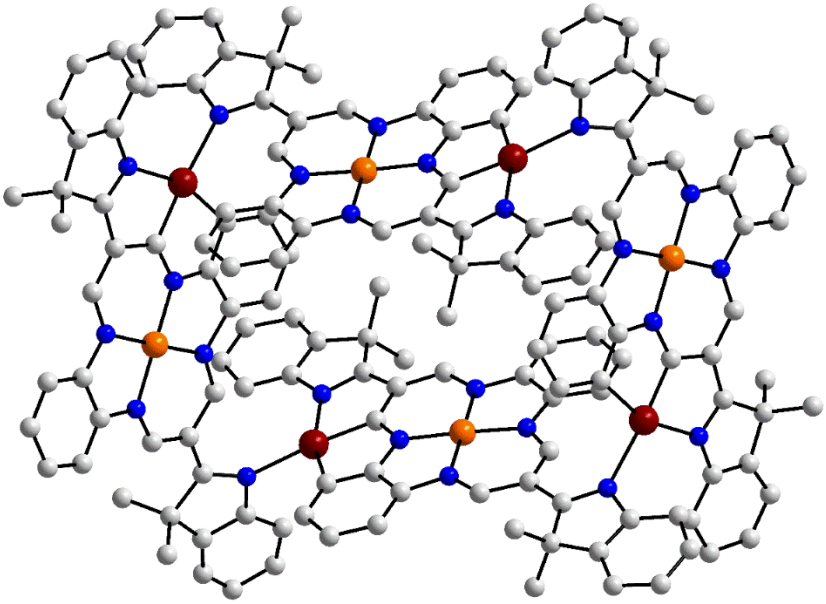

Figure 16. The molecular structure of octa-nuclear **80** comprising of alternating nickel(II) (orange spheres) and palladium(II) atoms.

In 2017, Yamashita *et al*. [78] synthesized two lanthanide(III) double-decker complexes by reacting ligand **69** with $Dy(acac)_3.6H_2O$ or $Tb(acac)_3.6H_2O$ at 220 ºC (Scheme 19). The complexes **81** and **82** were isolated in low yields after chromatographic purification. The crystal structures of **81** and **82** are isomorphous, with that of the former shown in Figure 17. The central atom is eight-coordinate being bound by two sets of core-N_4 atoms. The N_8 donor set defines a square anti-prismatic geometry. The electroneutrality of each complex is accomplished through the protonation of the nitrogen atom of an indolenine moiety. The magnetic susceptibility, χ values at room temperature for complexes **81** and **82** are 14.25 and 11.36 cm^3 K mol^{-1}, respectively. Both values decrease to 10.24 and 9.62 cm^3 K mol^{-1} at 2.0 K, which is ascribed to the depopulation of m_J sublevels of the ground state [78].

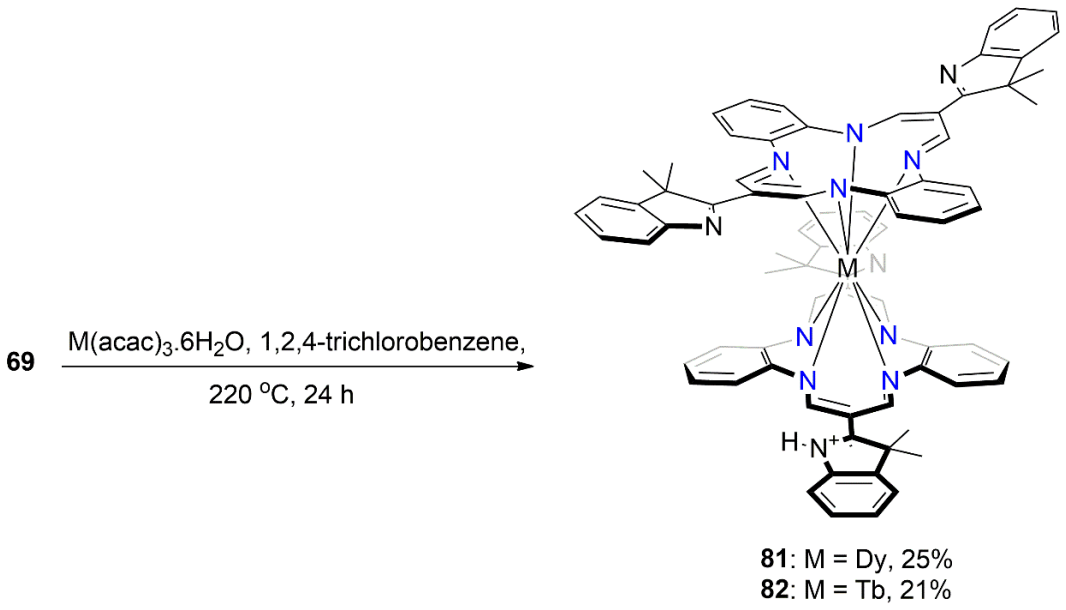

Scheme 19. Synthesis of dysprosium(III) and terbium(III) indoleninyl *meso*-substituted DBTAA complexes**, 81** and **82**.

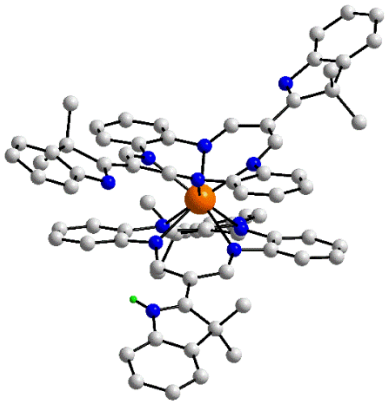

Figure 17. The molecular structure highlighting the square anti-prismatic geometry for the dysprosium(III) centre in **81**. Note the protonation of the indolenine-N atom to establish electroneutrality.

7. Synthesis and reactivity of *meso*-2-hydroxy-benzoyl-DBTAA

The starting material **83** was obtained from a non-template condensation reaction between 3-formylchromone and *o*-phenylenediamine [79]. The *O*-alkylation of **83** with 1,4-dibromobutane led to the intermediate **84a** (Scheme 20) [80]. A similar strategy was also reported for the decoration of **83** with various alkyl chains [81-86]. Next, a reaction of **84a** with

dimethylamine, followed by the addition of ammonium hexafluorophosphate gave strapped **84b** in 52% yield [80]. The co-facial dimeric **86** was synthesized from an alkylation reaction between **83** and **84a** in DMF over a week. On the other hand, the warm heating of **83** with intermediate **85** [81, 87] at 70 ºC afforded the non-symmetric dimer **87** in 37% yield. Further, the metalation of **86** with $Zn(OAc)_2$ afforded the complex **88** in 67% yield. Reaction of **87** with $Ni(OAc)_2.4H_2O$ led to the formation of *mono*-metalation complex **89** in moderate yield [88].

The UV-vis absorption spectrum of **84b** in DMSO demonstrates a slight red-shift upon the addition of small amounts of tetrabutylammonium fluoride or tetrabutylammonium hydroxide. Interestingly, the fluorescence spectrum shows an emission peak at 576 nm with an excitation peak at 380 nm. The changes in spectroscopic properties are due to the monodeprotonation of NH induced by F^- and OH^- anions [80]. On the other hand, the absorption spectrum of **88** shows a broad absorption profile between 300 to 450 nm, which corresponds to the π-π* transitions and charge-transfer (CT) transitions from metal to ligand [88].

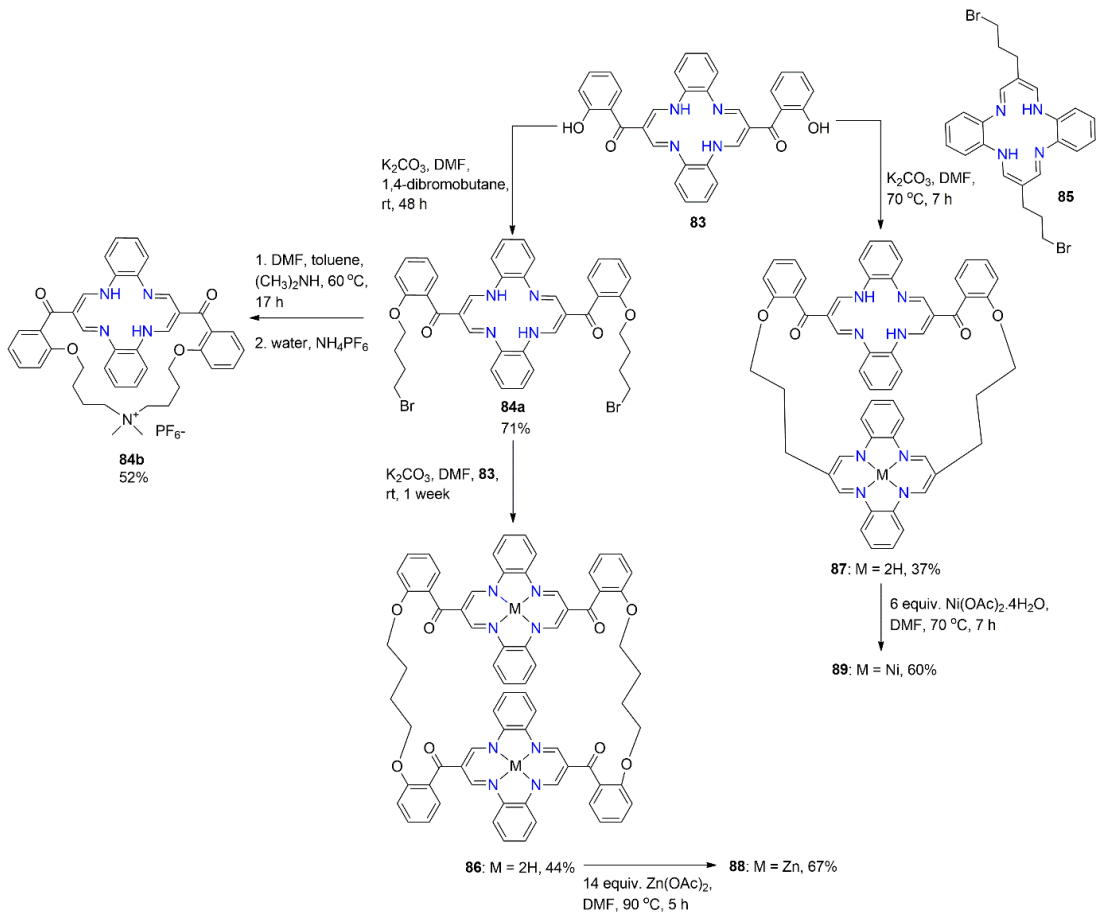

Scheme 20. Synthesis of strapped **84b** and dimeric complexes **88-89** benzoyl *meso*-substituted DBTAA.

Subsequently, the post-functionalization of the strapped, cyclic dimer of macrocycle DBTAA was reported by the same group. As illustrated in Scheme 21, precursor **90** was synthesized from the reaction of **83** with propargyl bromide in a mixture of K_2CO_3 and DMF. The central cavity of the precursor was then protected by performing a metalation reaction with $Zn(OAc)_2$ in hot DMF to afford **91** in excellent yield. Crystals of **91** were isolated as a 1:1 DMSO adduct, i.e. **91.DMSO** [89]. As shown in Figure 18a, the zinc(II) atom lies above the N_4 plane and the approximately square-pyramidal geometry is completed by an O-bound DMSO molecule in the apical position.

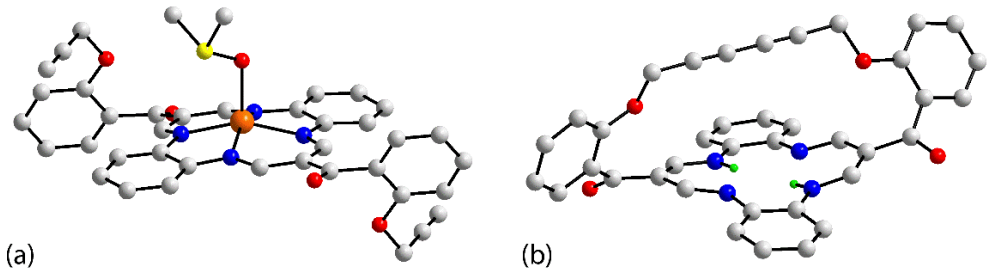

Figure 18. Molecular structures of (a) **91.DMSO** and (b) **92**.

The oxidative coupling of the terminal alkyne **91** under Glaser-Eglinton conditions, followed by a demetallation reaction afforded the strapped **92** and cyclic dimer **93** in 34 and 30% yields, respectively. The crystal structure of **92** is available and the molecular structure is illustrated in Figure 18b. The products were separated by column chromatography. Notably, compound **92** is present in a pair of racemic conformational enantiomers as determined by X-ray crystallography. Complexes **94** and **95** were achieved according to literature procedures [88]. The absorption spectrum of **90** shows an intense peak at 353 nm, which corresponds to the π-π* transition of the central core. In comparison, the electronic properties of **91** demonstrate a slight red-shift of 8 nm due to the alteration of the electronic distribution in the macrocyclic core upon the coordination by zinc(II). Moreover, the absorption spectra of **94** and **95** demonstrate a similar pattern to that of **91** [89].

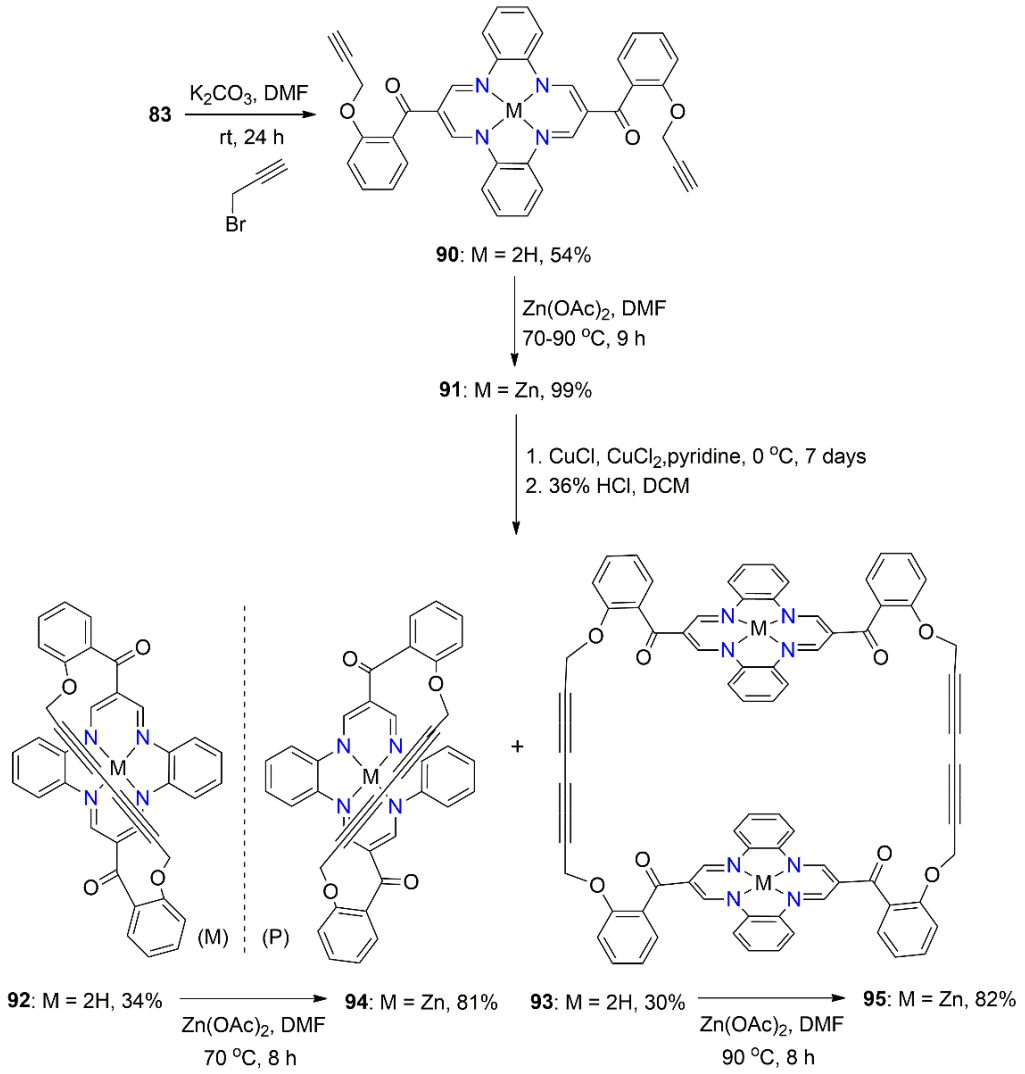

Scheme 21. Synthesis of strapped and cyclic dimer Zn(II) benzoyl *meso*-substituted DBTAA complexes, **94** and **95**. Please align the bonds at the top-right side of 94

The synthetic strategy was extended by synthesizing a DBTAA zinc(II) complex connected through a linear octane chain linker. The reaction was initiated by protecting one of the hydroxyl groups of **83** with a propargyl moiety (Scheme 22), as reported elsewhere [89]. The macrocycle **96** was stirred with 1,8-dibromooctane in a mixture of K_2CO_3 and DMF at room temperature for three days. Asymmetric **97** was isolated in 49% yield. The *O*-alkylation reaction between **96** and **97** again plays a key role in the formation of **98** in 47% yield. The ligand was then metallated with $Zn(OAc)_2$ to generate **99** in high yield. The absorption spectrum of **98** shows two intense peaks at 345 and 386 nm, which corresponds to the π-π* and n-π*(imine) transitions of the macrocycle, respectively [90]. This synthetic approach offers strong fundamental prospects for the construction of DNA/RNA binders and as anti-proliferative agents [12, 13, 83].

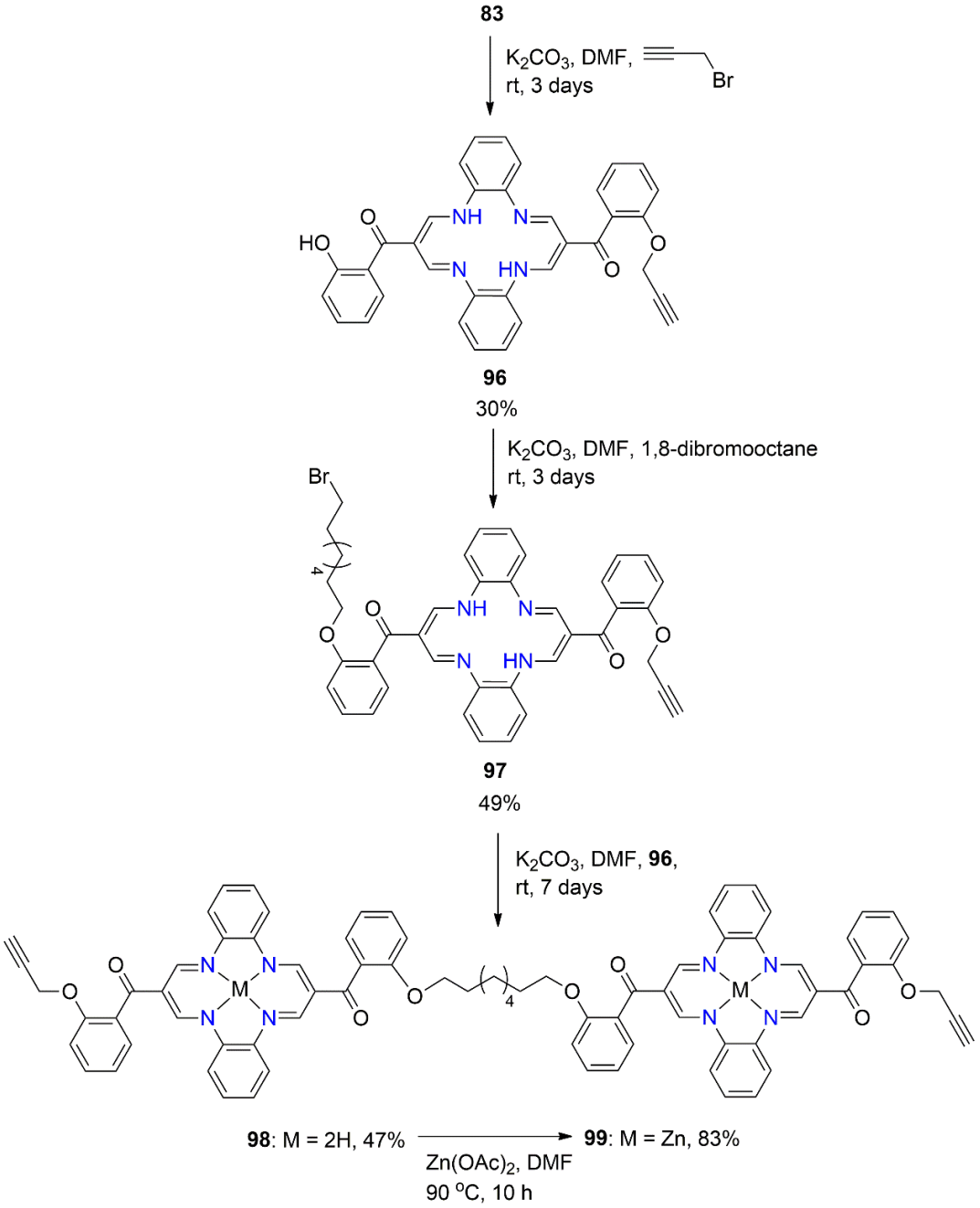

Scheme 22. Synthesis of dimeric zinc(II) benzoyl *meso*-substituted DBTAA complex **99**.

Conclusions

In summary, synthetic methodologies, structural chemistry and key spectroscopic properties of functionalized DBTAA derivatives developed over the past decade have been reviewed. The synthesis of DBTAA derivatives is still a challenging task owing to the limited synthetic options, poor stability and poor solubility of the products. The coordination modes of the actinide and lanthanide metals towards DBTAA-derived ligands are interesting and exhibit distinctive molecular models compared to that exhibited by transition metals. The attractive UV-vis absorption properties of the DBTAA derivatives could be utilized in various optoelectronic devices. Extensive efforts are required to develop new synthetic innovations to functionalize the macrocycle core, as well as to develop future applications in materials science and optoelectronics.

Declaration of competing interest

There are no conflicts of interest to declare.

Acknowledgement

The authors gratefully acknowledge Sunway University Sdn Bhd (Grant no. GRTIN-RRO-56-2022) for support of structural studies.

References

[1] P. Mountford, Chem. Soc. Rev. 27 (1998) 105-116.

[2] F.A. Cotton, J. Czuchajowska, Polyhedron 9 (1990) 2553-2566.

[3] A.Q. Ramle, H. Khaledi, A.H. Hashim, M.A. Mingsukang, A.K. Mohd Arof, H.M. Ali, W.J. Basirun, Dyes Pigm. 164 (2019) 112-118.

[4] R. Sustmann, H.-G. Korth, D. Kobus, J. Baute, K.-H. Seiffert, E. Verheggen, E. Bill, M. Kirsch, H. de Groot, Inorg. Chem. 46 (2007) 11416-11430.

[5] J. Paschke, M. Kirsch, H.-G. Korth, H. de Groot, R. Sustmann, J. Am. Chem. Soc. 123 (2001) 11099-11100.

[6] A.M. Whyte, Y. Shuku, G.S. Nichol, M.M. Matsushita, K. Awaga, N. Robertson, J. Mater. Chem. 22 (2012) 17967-17975.

[7] X. Shen, N. Liu, K. Utsunomiya, L. Sun, B.-K. Jiang, X. Wang, Y.-Q. Yang, Y. Xu, K. Sakata, D.-R. Zhu, J. Inorg. Organomet. Polym. Mater. 21 (2011) 91-96.

[8] X. Wang, X. Shen, Y.-J. Zhang, F. Su, G. Liu, Y. Xu, D.-R. Zhu, Inorg. Chem. Commun. 35 (2013) 45-49.

[9] P. Zhao, C. Zhong, L. Hunag, L. Niu, F. Zhang, Corros. Sci. 50 (2008) 2166-2171.

[10] M. Yamana, H. Shinozaki, N. Kashiwazaki, Sens. Actuators B Chem. 66 (2000) 299-302.

[11] Z. Liang, T. Zhang, P. Cao, T. Yoshida, W. Tang, X. Wang, Y. Zuo, P. Tang, M. Heggen, R.E. Dunin-Borkowski, J.R. Morante, A. Cabot, M. Yamashita, J. Arbiol, Chem. Eng. J. 442 (2022) 136129.

[12] M.R. Stojković, M. Marjanović, D. Pawlica, L. Dudek, J. Eilmes, M. Kralj, I. Piantanida, New J. Chem. 34 (2010) 500-507.

[13] M.R. Stojković, I. Piantanida, M. Kralj, M. Marjanović, M. Žinić, D. Pawlica, J. Eilmes, Bioorg. Med. Chem. 15 (2007) 1795-1801.

[14] M. Luo, X.-H. Zhang, D.J. Darensbourg, Macromolecules 48 (2015) 6057-6062.

[15] S. Tian, Q. Yang, S. Mohsen Sadeghzadeh, Inorg. Chem. Commun. 125 (2021) 108441.

[16] A. Chirila, K.M. van Vliet, N.D. Paul, B. de Bruin, Eur. J. Inorg. Chem. 2018 (2018) 2251-2258.

[17] A. Chirila, B. Gopal Das, N.D. Paul, B. de Bruin, ChemCatChem 9 (2017) 1413-1421.

[18] B.G. Das, A. Chirila, M. Tromp, J.N.H. Reek, B. de Bruin, J. Am. Chem. Soc. 138 (2016) 8968-8975.

[19] J.U. Franco, J.C. Hammons, D. Rios, M.M. Olmstead, Inorg. Chem. 49 (2010) 5120-5125.

[20] P.C. Andrews, J.L. Atwood, L.J. Barbour, P.J. Nichols, C.L. Raston, Chem. Eur. J. 4 (1998) 1384-1387.

[21] B. Korybut-Daszkiewicz, R. Bilewicz, K. Woźniak, Coord. Chem. Rev. 254 (2010) 1637-1660.

[22] T.F. Higgins, S. Lee, J.D. Winkler, J. Org. Chem. 86 (2021) 5417-5422.

[23] J. Chen, N. Ye, N.W. Alcock, D.H. Busch, Inorg. Chem. 32 (1993) 904-910.

[24] M.D. Walter, R. Fandos, R.A. Andersen, New J. Chem. 30 (2006) 1065-1070.

[25] G.H. Imler, S. Bhagan, V.L. Coffin, B.B. Wayland, Inorg. Chem. 51 (2012) 3352-3354.

[26] M.C. Weiss, G. Gordon, V.L. Goedken, Inorg. Chem., 16 (1977) 305-310.

[27] L. Dey, S. Rabi, Z.A. Begum, T. Takase, I.M.M. Rahman, E.R.T. Tiekink, T.G. Roy, Z. Kristallogr. NCS 236 (2021) 1121-1124.

[28] L. Pilia, Y. Shuku, S. Dalgleish, K. Awaga, N. Robertson, ACS Omega 3 (2018) 10074-10083.

[29] E.-G. Jäger, Z. Anorg. Allg. Chem. 364 (1969) 177-191.

[30] A.R. Cutler, D. Dolphin, J. Coord. Chem. 6 (1976) 59-61.

[31] A.R. Cutler, C.S. Alleyne, D. Dolphin, Inorg. Chem. 24 (1985) 2276-2281.

[32] Y. Jiang, I. Oh, S.H. Joo, O. Buyukcakir, X. Chen, S.H. Lee, M. Huang, W.K. Seong, S.K. Kwak, J.-W. Yoo, R.S. Ruoff, J. Am. Chem. Soc. 141 (2019) 16884-16893.

[33] X. Shen, L. Sun, B.-K. Jiang, X. Wang, A. Nakashima, N. Miyamoto, K. Sakata, Y. Xu, D.-R. Zhu, Inorg. Chem. Commun. 14 (2011) 1555-1560.

[34] Sweety, V.K. Vashistha, A. Kumar, R. Singh, Russ. J. Electrochem. 55 (2019) 161-167.

[35] A.M. Mehranpour, S. Hashemnia, E. Bashiri, Synth. Commun. 43 (2013) 1931-1938.

[36] C.L. Honeybourne, P. Burchill, M.K. Yoo, G.R. Brubaker, Nontemplate Syntheses of Complexes with Conjugated Mackocyclic Ligands, in: Inorg. Synth. 1978, pp. 44-49.

[37] A.M. Mehranpour, S. Hashemnia, J. Ameri Rad, J. Heterocycl. Chem. 50 (2013) 821-827.

[38] A.M. Mehranpour, S. Hashemnia, E. Bashiri, J. Heterocycl. Chem. 53 (2016) 958-962.

[39] W.J. Belcher, P.J. Brothers, M.V. Land, C.E.F. Rickard, D.C. Ware, J. Chem. Soc. Dalton Trans. (1993) 2101-2105.

[40] K. Brandenburg, DIAMOND. Visual Crystal Structure Information System, version 3.1, Crystal Impact, Bonn, Germany, 2006.

[41] E.M. Goggins, T.T. Lekich, W.W. Weare, R.D. Sommer, M.A. Ribeiro, C.B. Pinheiro, Eur. J. Inorg. Chem. 2016 (2016) 1054-1059.

[42] V.L. Goedken, J.A. Ladd, J. Chem. Soc Chem. Commun. (1982) 142-144.

[43] C.-H. Yang, J.A. Ladd, V.L. Goedken, J. Coord. Chem. 19 (1988) 235-251.

[44] U.J. Williams, B.D. Mahoney, P.T. DeGregorio, P.J. Carroll, E. Nakamaru-Ogiso, J.M. Kikkawa, E.J. Schelter, Chem. Commun. 48 (2012) 5593-5595.

[45] U.J. Williams, B.D. Mahoney, A.J. Lewis, P.T. DeGregorio, P.J. Carroll, E.J. Schelter, Inorg. Chem. 52 (2013) 4142-4144.

[46] D.C. Bradley, J.S. Ghotra, F.A. Hart, J. Chem. Soc. Dalton Trans. (1973) 1021-1023.

[47] G.H. Imler, M.J. Zdilla, B.B. Wayland, Inorg. Chem. 52 (2013) 11509-11513.

[48] G.H. Imler, M.J. Zdilla, B.B. Wayland, J. Am. Chem. Soc. 136 (2014) 5856-5859.

[49] G.H. Imler, G.M. Peters, M.J. Zdilla, B.B. Wayland, Inorg. Chem. 54 (2015) 273-279.

[50] R. Fandos, M.D. Walter, D. Kazhdan, R.A. Andersen, Organometallics 25 (2006) 3678-3687.

[51] R. Fandos, S.S. Rozenel, R.A. Andersen, Polyhedron 137 (2017) 17-23.

[52] S. Hohloch, M.E. Garner, B.F. Parker, J. Arnold, Dalton Trans. 46 (2017) 13768-13782.

[53] S. De Angelis, E. Solari, E. Gallo, C. Floriani, A. Chiesi-Villa, C. Rizzoli, Inorg. Chem. 31 (1992) 2520-2527.

[54] T. Cantat, B.L. Scott, J.L. Kiplinger, Chem. Commun. 46 (2010) 919-921.

[55] D. Patel, A.J. Wooles, E. Hashem, H. Omorodion, R.J. Baker, S.T. Liddle, New J. Chem. 39 (2015) 7559-7562.

[56] M.J. Monreal, R.K. Thomson, T. Cantat, N.E. Travia, B.L. Scott, J.L. Kiplinger, Organometallics 30 (2011) 2031-2038.

[57] S. Hohloch, M.E. Garner, C.H. Booth, W.W. Lukens, C.A. Gould, D.J. Lussier, L. Maron, J. Arnold, Angew. Chem. Int. Ed. 57 (2018) 16136-16140.

[58] E.A. Pedrick, M.K. Assefa, M.E. Wakefield, G. Wu, T.W. Hayton, Inorg. Chem. 56 (2017) 6638-6644.

[59] D.M. Barnhart, C.J. Burns, N.N. Sauer, J.G. Watkin, Inorg. Chem. 34 (1995) 4079-4084.

[60] M.K. Assefa, E.A. Pedrick, M.E. Wakefield, G. Wu, T.W. Hayton, Inorg. Chem. 57 (2018) 8317-8324.

[61] M.P. Wilkerson, C.J. Burns, R.T. Paine, B.L. Scott, Inorg. Chem. 38 (1999) 4156-4158.

[62] R. Kia, M. Hosseini, A. Abdolrahimi, M. Mahmoudi, CrystEngComm 21 (2019) 5222-5226.

[63] Y. Shen, H. Xue, Y.-Q. Wei, M. Shen, R.-C. Xu, X. Wang, X. Shen, D.-R. Zhu, J. Incl. Phenom. Macrocycl. Chem. 86 (2016) 191-199.

[64] J.A. Paquette, E.R. Sauvé, J.B. Gilroy, Macromol. Rapid Commun. 36 (2015) 621-626.

[65] J.A. Paquette, J.B. Gilroy, J. Polym. Sci. Part A: Polym. Chem. 54 (2016) 3257-3266.

[66] H.-H. Huang, C.-G. Chao, S.-L. Lee, H.-J. Wu, C.-h. Chen, T.-Y. Luh, Org. Biomol. Chem. 10 (2012) 5948-5953.

[67] J.A. Paquette, A. Rabiee Kenaree, J.B. Gilroy, Polym. Chem. 8 (2017) 2164-2172.

[68] C. Reichardt, W. Scheibelein, Z. Naturforsch. B 33 (1978) 1012-1015.

[69] J.E. Beves, B.E. Chapman, P.W. Kuchel, L.F. Lindoy, J. McMurtrie, M. McPartlin, P. Thordarson, G. Wei, Dalton Trans. (2006) 744-750.

[70] H. Ryu, Y. Mulyana, I.-H. Park, J. Kim, L.F. Lindoy, S.S. Lee, CrystEngComm 17 (2015) 5717-5724.

[71] Y. Mulyana, L.F. Lindoy, C.J. Kepert, J. McMurtrie, A. Parkin, P. Turner, G. Wei, J.G. Wilson, J. Incl. Phenom. Macrocycl. Chem. 71 (2011) 455-462.

[72] H. Khaledi, M.M. Olmstead, H. Mohd Ali, N.F. Thomas, Inorg. Chem. 52 (2013) 1926-1941.

[73] A.Q. Ramle, A. Karakas, A.K.M. Arof, M. Karakaya, M. Taser, A. Gozutok, C. Chin Fei, N.M. Julkapli, W.J. Basirun, J. Heterocycl. Chem. 57 (2020) 3566-3573.

[74] A. Minsky, A.Y. Meyer, R. Poupko, M. Rabinovitz, J. Am. Chem. Soc. 105 (1983) 2164-2172.

[75] H. Rabaâ, H. Khaledi, M.M. Olmstead, D. Sundholm, J. Phys. Chem. A 119 (2015) 5189-5196.

[76] K. Sakata, M. Shimoda, M. Hashimoto, J. Heterocycl. Chem. 33 (1996) 1593-1598.

[77] H. Khaledi, M.M. Olmstead, T. Fukuda, H. Mohd Ali, Inorg. Chem. 53 (2014) 11348-11350.

[78] Z. Liang, M. Damjanović, M. Kamila, G. Cosquer, B.K. Breedlove, M. Enders, M. Yamashita, Inorg. Chem. 56 (2017) 6512-6521.

[79] I. Sigg, G. Haas, T. Winkler, Helv. Chim. Acta 65 (1982) 275-279.

[80] Ł. Dudek, J. Grolik, A. Kaźmierska, E. Szneler, A. Eilmes, K. Stadnicka, J. Eilmes, Tetrahedron Lett. 52 (2011) 3597-3601.

[81] A. Kaźmierska, M. Gryl, K. Stadnicka, L. Sieroń, A. Eilmes, J. Nowak, M. Matković, M. Radić-Stojković, I. Piantanida, J. Eilmes, Tetrahedron 71 (2015) 4163-4173.

[82] J. Grolik, K. Zwoliński, L. Sieroń, J. Eilmes, Tetrahedron 67 (2011) 2623-2632.

[83] M. Radić Stojković, M. Škugor, S. Tomić, M. Grabar, V. Smrečki, Ł. Dudek, J. Grolik, J. Eilmes, I. Piantanida, Org. Biomol. Chem. 11 (2013) 4077-4085.

[84] M.R. Stojković, M. Škugor, Ł. Dudek, J. Grolik, J. Eilmes, I. Piantanida, Beilstein J. Org. Chem. 10 (2014) 2175-2185.

[85] K.M. Zwoliński, J. Eilmes, Beilstein J. Org. Chem. 15 (2019) 617-622.

[86] D. Pawlica, M. Radić-Stojković, Ł. Dudek, I. Piantanida, L. Sieroń, J. Eilmes, Tetrahedron 65 (2009) 3980-3989.
[87] R. Hanke, E. Breitmaier, Chem. Ber. 115 (1982) 1657-1661.
[88] K.M. Zwoliński, J. Eilmes, Chem. Commun. 52 (2016) 4084-4087.
[89] K.M. Zwoliński, L. Sieroń, J. Eilmes, Org. Chem. Front. 5 (2018) 171-178.
[90] K.M. Zwoliński, J. Eilmes, Org. Biomol. Chem. 16 (2018) 5508-5516.